

Review

Ten Years Milestones in Xanthine Oxidase Inhibitors Discovery: Febuxostat-Based Inhibitors Trends, Bifunctional Derivatives, and Automatized Screening Assays

Miguel F. S. de Abreu¹, Camila A. Wegermann^{1,2}, Millena S. Ceroullo¹, Isabella G. M. Sant'Anna¹ and Renato C. S. Lessa^{1,*} 

¹ Departamento de Química Orgânica, Campus do Valonguinho, Instituto de Química, Universidade Federal Fluminense, Niterói 24020-150, Brazil

² Departamento de Química Inorgânica, Campus do Valonguinho, Instituto de Química, Universidade Federal Fluminense, Niterói 24020-150, Brazil

* Correspondence: renatolessa@id.uff.br

Abstract: Xanthine oxidase (XO) is an enzyme involved in the oxidative process of hypoxanthine and xanthine to uric acid (UA). This process also produces reactive oxygen species (ROS) as byproducts. Both UA and ROS are dangerous for human health, and some health conditions trigger upregulation of XO activity, which results in many diseases (cancer, atherosclerosis, hepatitis, gout, and others) given the worsened scenario of ROS and UA overproduction. So, XO became an attractive target to produce and discover novel selective drugs based on febuxostat, the most recent XO inhibitor out of only two approved by FDA. Under this context, high-performance liquid chromatography (HPLC) and capillary electrophoresis (CE) have been successfully applied to rapidly and easily screen for bioactive compounds, isolated or in complex natural matrixes, that act as enzyme inhibitors through the use of an immobilized enzyme reactor (IMER). This article's goal is to present advances comprising febuxostat-based XO inhibitors as a new trend, bifunctional moieties capable of inhibiting XO and modulating ROS activity, and in-flow techniques employing an IMER in HPLC and CE to screen for synthetic and natural compounds that act as XO inhibitors.

Keywords: enzyme inhibition; drug development; drugs screening; allopurinol; febuxostat; Y-700; topiroxostat; isostere; nanomolar; ROS



Citation: de Abreu, M.F.S.; Wegermann, C.A.; Ceroullo, M.S.; Sant'Anna, I.G.M.; Lessa, R.C.S. Ten Years Milestones in Xanthine Oxidase Inhibitors Discovery: Febuxostat-Based Inhibitors Trends, Bifunctional Derivatives, and Automatized Screening Assays. *Organics* **2022**, *3*, 380–414. <https://doi.org/10.3390/org3040026>

Academic Editors: Wim Dehaen, Michal Szostak and Huaping Xu

Received: 23 July 2022

Accepted: 28 September 2022

Published: 10 October 2022

Publisher's Note: MDPI stays neutral with regard to jurisdictional claims in published maps and institutional affiliations.

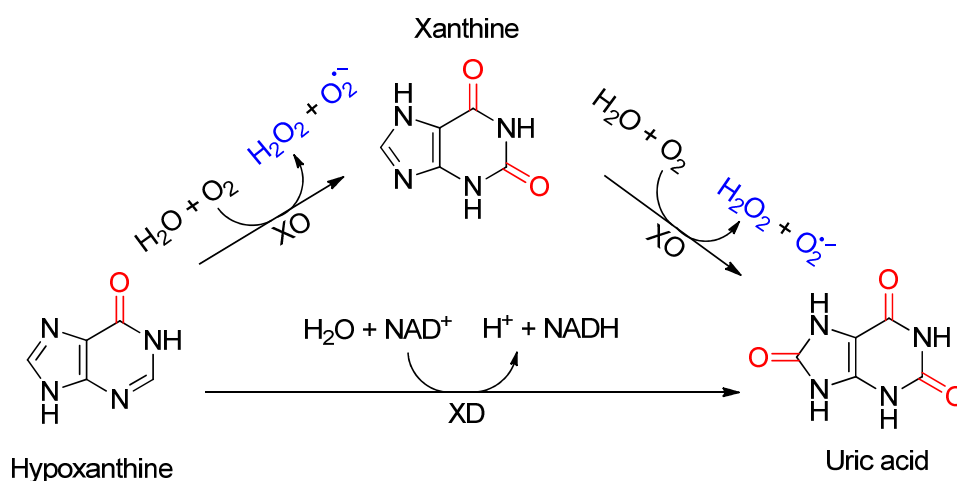


Copyright: © 2022 by the authors. Licensee MDPI, Basel, Switzerland. This article is an open access article distributed under the terms and conditions of the Creative Commons Attribution (CC BY) license (<https://creativecommons.org/licenses/by/4.0/>).

1. Introduction

The enzymes xanthine oxidase (XO) and xanthine dehydrogenase (XD) are interconvertible forms of the homodimer enzyme xanthine oxidoreductase (XOR) [1]. XOR is a cytosolic located enzyme distributed in many animal species, especially humans, which is the principal species of interest when considering medicinal chemistry and the development of novel drugs for better living conditions. The XO form belongs to the mononuclear molybdenum family of enzymes [2] and will be the focus of this review. It plays a key role as an oxidizing catalyst against many molecules like purines, pterins, heterocycles, and aldehydes. Therefore, it operates as a regulating agent for endogenous compounds and xenobiotics by activating or detoxifying them [3].

Despite XO and XD producing uric acid (UA) as a product from the substrate hypoxanthine, a remarkable difference between them centers around the chemical species involved in the catalytic process. While XD mediated catalysis centers around harmless to tolerable species (NAD⁺, NADH, oxygen, and water) during the redox process, XO produces harmful species known as reactive oxygen species (ROS), such as H₂O₂ and superoxide radical as byproducts (Scheme 1) [3].



Scheme 1. XO and XD enzymatic reactions.

Unfortunately, tissue damage [4], hemolytic diseases like malaria [5], sepsis [6] and thalassemia [7], acute respiratory distress syndrome [8], chronic obstructive pulmonary disease [9] and codeine-based treatments [10] lead to upregulated XO levels or activity, resulting in overproduction of UA and ROS. As examples, an over 6-fold increase in XO level was observed in patients under several malaria condition [5] and an almost 3-fold increase in XO activity was observed in chronic obstructive pulmonary disease [9].

The accumulation of UA leads to hyperuricemia, a stage achieved by concentrations above 6 mg/dL of serum uric acid levels. That results in gout and arthritis, a condition where uric acid crystals are formed in the joints. It may extend to the urogenital system through the formation of stones, leading to nephrolithiasis or crystalluria [11]. Moreover, there is still a debate about whether hyperuricemia is correlated to cardiovascular diseases and if XO inhibitors can be employed to lower cardiovascular disease incidents [12–15]. On the other hand, carbohydrates, deoxyribonucleic acid (DNA), proteins, amino acids, and lipids are species that are reactive through oxidative species, specifically ROS. Therefore, the production of abnormal levels of ROS is a major threat to any human due to the development of many abnormal conditions, including: hepatitis, cancer, inflammation, aging, ischemia, cardiovascular disease, and endothelial and organ dysfunction [5,7,14,16–18].

The search for drugs that act as enzyme inhibitors is advantageous given the selective characteristic of the inhibitor–substrate interaction. The facile interaction between small molecules and enzymes usually leads to high druggability, which means valid interaction between the target (enzyme) with the drug as predicted or expected, reducing collateral effects due to undesired interactions with other pharmacophoric sites [19]. That selective interaction turned out to be an outstanding target to probe novel potential bioactive compounds via immobilized enzyme reactors (IMERs) once it is fully compatible with high precision techniques, for this article’s specific discussion: high-performance liquid chromatography (HPLC) and capillary electrophoresis (CE) [20–24].

Based on the aforementioned, it becomes specifically interesting to invest in XO inhibitors synthesis and screening, once the only FDA-approved inhibitors are allopurinol and febuxostat. Moreover, pyrazolopyrimidine-based inhibitors (an allopurinol-based scaffold) may experience inhibition resistance by XO involved in pathogenic function, which encourages searching for allopurinol substitutes [7,25].

In the following sections, advances comprising the obtainment of novel non-allopurinol-based XO inhibitors will be presented, highlighting the promising results of each work (Section 3). Then, high-performance liquid chromatography (HPLC) and capillary electrophoresis (CE) developments comprising the use of an immobilized enzyme reactor (IMER) for the identification of XO inhibitors will be presented (Section 4).

2. Methods

To gather the articles for this paper, Google Scholar, Scifinder platform, Web of Science, and PubMed were used. For general reference about XO and in-flow assays, papers in English without a publication time restriction were considered, given that many early 1990s and 2000s works are important for the discussions. However, only articles published in English between 2012–2022 were considered to present the developments in Sections 3 and 4. The selected keyword for the initial search was “xanthine oxidase inhibitors”. For the scope of this work, patents were not considered. Articles describing the synthesis protocol of the in-flow screened derivatives as XO inhibitors were fully discussed, one time only, in the section on screening methods (Section 4), to keep the work’s ideas condensed. Systematic descriptions of the synthetical approaches were not done, but the synthesis steps were fully presented through the schemes, to keep the focus of the article’s discussion on the compound’s biological activity towards XO inhibition.

3. XO Inhibitors

Since the late 1960s Allopurinol (Figure 1), the functional isomer of hypoxanthine, has been the most viable purinergic inhibitor of XO for human use. It behaves as a suicidal competitive, to xanthine, inhibitor that binds to the molybdenum center of XO [26]. Despite the molecular deviations approach in medicinal chemistry that puts allopurinol’s success as a XO inhibitor ahead when considering rational drug design, some works describe promising advances regarding different molecular frameworks.

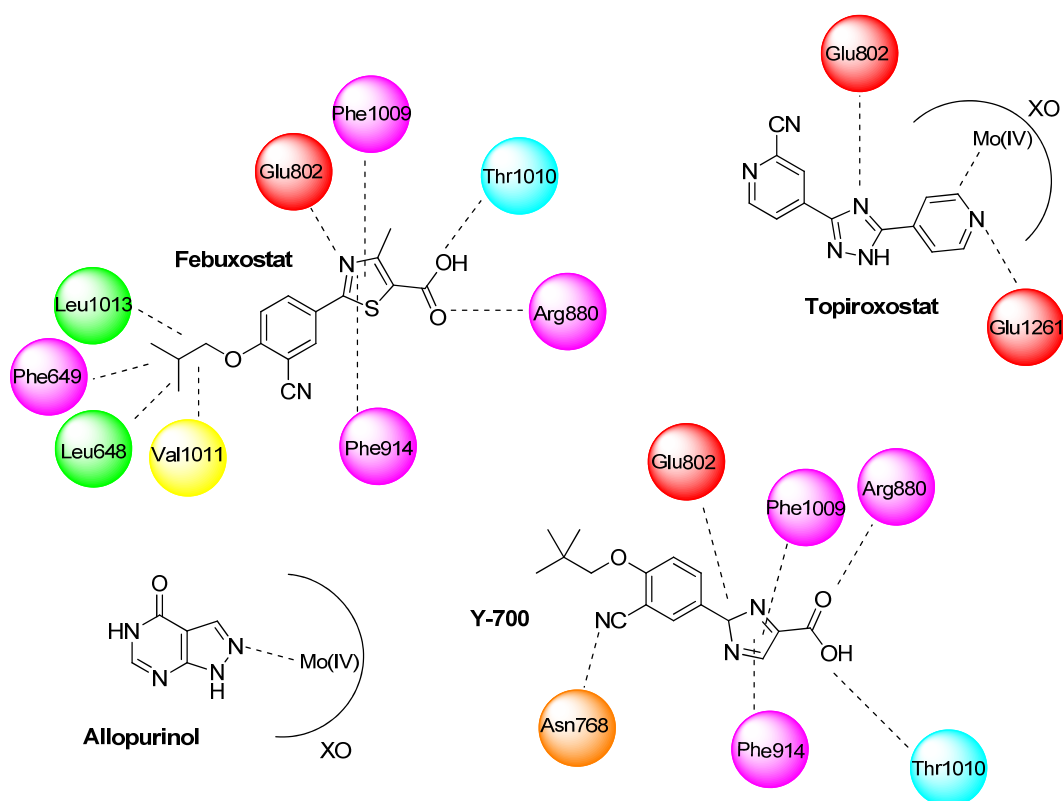


Figure 1. Allopurinol, febuxostat, topiroxostat and Y-700 molecular structures and docking sites.

The 2-[3-cyano-4-(2-methylpropoxy)phenyl]-4-methylthiazole-5-carboxylic acid marketed as febuxostat (Figure 1) is a non-purine urate-lowering drug used as an alternative to allopurinol for treatment of hyperuricemia in gout. This compound was studied as a XO inhibitor in chimpanzees [27] and in rodents [28], and its action is related to the inhibition of both oxidized and reduced forms of XO febuxostat, which was approved for gouty arthritis by Europe in 2008 and by the FDA in 2009 [29,30].

Febuxostat is a non-competitive inhibitor and blocks the active site of the protein through important residual interactions. The oxygen atoms of the carboxylate group interact with the residues Thr1010 and Arg880 through hydrogen bonds, while the Glu802 also forms a hydrogen bond with the probably protonated thiazole nitrogen. Another interaction ensures the proper orientation of the molecule into the narrow channel of the enzyme such as the hydrophobic interactions of the 4-isobutoxy tail with the amino acids Leu648, Phe649, Val1011, and Leu1013, and aromatic interactions of the sandwiched thiazole ring with the Phe914 and Phe1009 [31].

An important analog of febuxostat is Y-700, 1-(3-cyano-4-neopentyloxyphenyl)pyrazole-4-carboxylic acid (Figure 1), a mixed-type inhibitor developed and studied by Fukunari and coworkers [32] and Ishibuchi and coworkers [33]. This compound features excellent inhibition activity and in vivo distinct hypouricemic effect. A crystallographic analysis between the Y-700 and XO active site shows similar interactions observed in febuxostat like electrostatic interaction between the carboxyl oxygen with Agr880; cyano group and Asn768; and H-bonds between the carboxyl and Thr1010 residue. The pyrazole ring interacts with Glu802 and is sandwiched by Phe914 and Phe1009, among other hydrophobic interactions [32].

Topiroxostat (Figure 1), known as FYX-051 or 4-[5-(Pyridin-4-yl)-1*H*-1,2,4-triazol-3-yl]pyridine-2-carbonitrile, is a potent XOR inhibitor approved in Japan for the treatment of hyperuricemia in 2013 [34]. Its structure is a hybrid between pyridine and cyanopyridine moieties linked by a triazole nucleus to [35]. Topiroxostat displays a hybrid type inhibition comprising an initial competitive inhibition followed by a covalent linkage through a complex formation between the oxygen-molybdenum (IV) and its hydroxylated intermediary, Glu802 and Glu1261 residues [36,37].

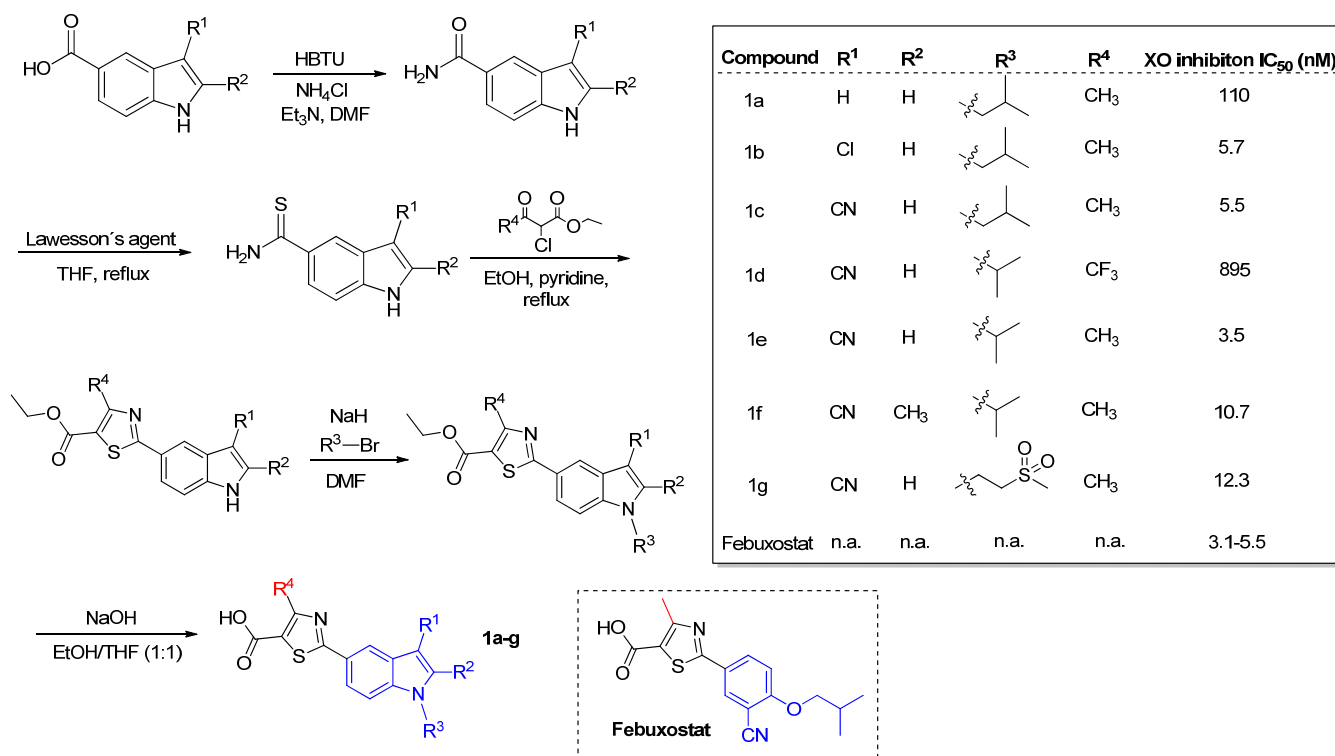
Since then, efforts to discover novel non-allopurinol-based XO inhibitors have been made through the synthesis of febuxostat, the most recent, out of a total of two, FDA approved drug for XO inhibition, analogs aiming to improve the interaction modes with the active site of XO and consequently, the inhibition activity.

3.1. Febuxostat-Based XO Inhibitors

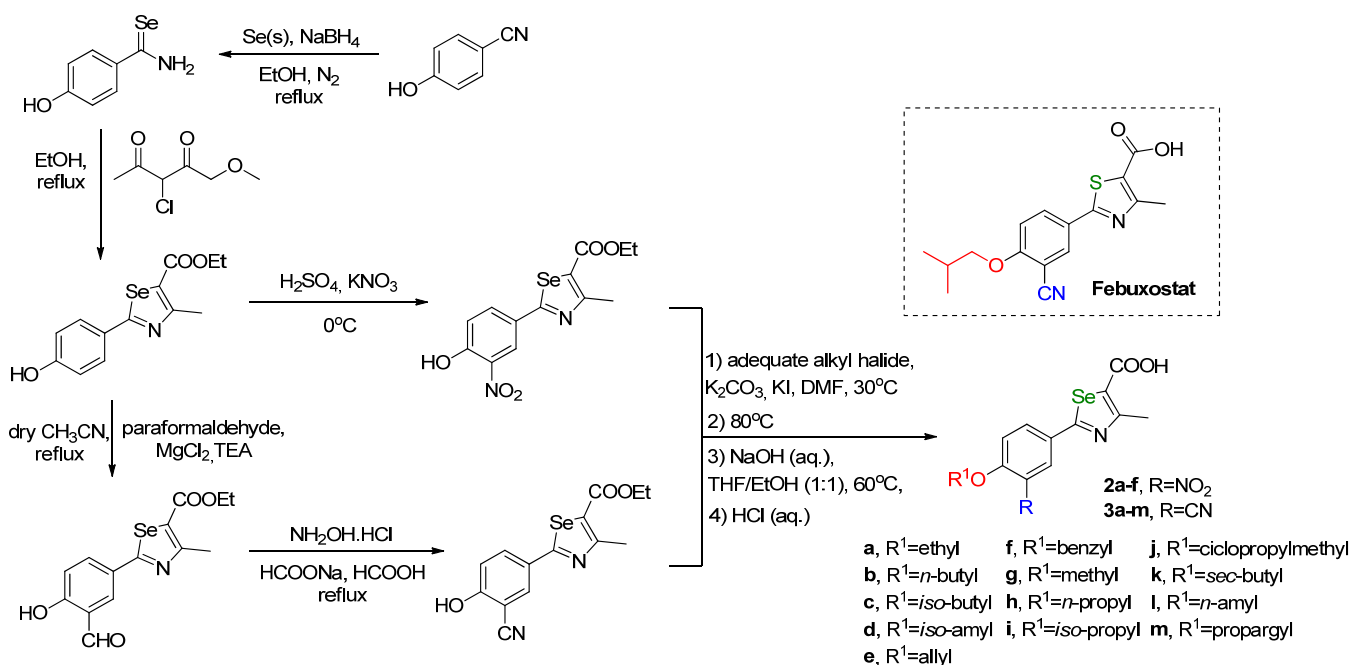
3.1.1. Derivatives Based on Five-Member Heterocyclic Rings

Focusing on a structure activity relationship (SAR) analysis, a library of more than twenty hybrid structures of indolethiazoles with four different substituents were explored as XO inhibitors and urate-lowering activity in rats by Song and coworkers, of which we highlight the selected examples **1a–g** (Scheme 2) [38]. Firstly, it was shown that electron-withdrawing substituents at the R¹-position favor XO inhibition. While at the R⁴-position, it harshly decreases. The activity of the molecule is also favored with hydrophobic substituents at the R³-position and without steric hindrance between R²-R³-positions. The best compound tested (**1e**) also showed a uric acid inhibition of 60% at 1 h (10 mg/kg) in rats, beyond the excellent in vitro IC₅₀ of 3.5 nM, comparable to febuxostat. The other derivatives also reached nanomolar IC₅₀ values. A docking analysis shows the same interactions of the carboxylate moiety and the thiazole ring that occurs with febuxostat. Despite the replacement of the phenyl group by an indole group, the cyano moiety was able to form hydrogen bonds with an Asn768 residue.

The replacement of the sulfur atom by a selenium one, in a series of febuxostat derivatives, **2a–f** and **3a–m** (Scheme 3), revealed an improvement in the inhibition potential of XO with in vitro IC₅₀ values in nanomolar ranges (same as febuxostat), as observed by Guan and coworkers (Table 1) [39]. The most potent XO inhibitor (**3e**) was compared with febuxostat (IC₅₀ of 18.6 nM), showing a better performance with an in vitro IC₅₀ value of 5.5 nM. Interestingly, its non-hydrolyzed precursor (not represented) did not present any activity at the tested concentration of 10 μM. Despite the size difference between sulfur and selenium atoms, a docking analysis showed similar interactions with the XO active site and a good overlap of the molecules. The kinetics analysis for **3e** showed a mixed-type inhibition.



Scheme 2. Synthesis of the indolethiazoles selected examples **1a–g** analogs of febuxostat and its *in vitro* XO inhibition potential in terms of IC₅₀ [38]. HBTU = Hexafluorophosphate Benzotriazole Tetramethyl Uronium.



Scheme 3. Synthesis of selenazole derivatives **2a–f** and **3a–m** [39].

Table 1. Selenazole derivatives **2a–f** and **3a–m** in vitro XO inhibition potential in terms of IC₅₀ [39].

Compound	IC ₅₀ (nM)	Compound	IC ₅₀ (nM)	Compound	IC ₅₀ (nM)
2a	82.5	3b	13.2	3i	15.7
2b	49.2	3c	9.1	3j	13.3
2c	33.7	3d	29.2	3k	10.4
2d	65.6	3e	5.5	3l	45.6
2e	16.1	3f	35.4	3m	53.8
2f	40.3	3g	30.6	Febuxostat	18.6
3a	24.8	3h	16.2		

Other two classes (CI = **4a–e**, **5a–e**, and CII = **6a–f**, **7f,g**, **8f,g**) of Febuxostat analogs were synthesized by Jing Li and coworkers [40] to explore the isosteric replacement of the thiazole ring with a pyrazole ring (Scheme 4). Modifications between class I and II were mainly centered on phenyl substituents (-OR for CI and -NR for CII) for SAR studies. For CI class, substituents at R¹ proved to be inefficient for the inhibition effect, once the derivatives did not show significant activity for the tested concentration (Table 2). While for CII, the general observed IC₅₀ values were comparable to febuxostat when R¹ = H. Moreover, for the most potent compound, **6f** (IC₅₀ = 4.2 nM), molecular modeling showed similar interactions with the XO active site as well as Y-700 and febuxostat. Additionally, the pyrazole ring, as with the thiazole ring in febuxostat, exhibits aromatic interactions with Phe914 and Phe1009. Studies in vivo have shown that oral administration of **6f** reduced serum uric acid levels in hyperuricemic mice with a similar profile of febuxostat.

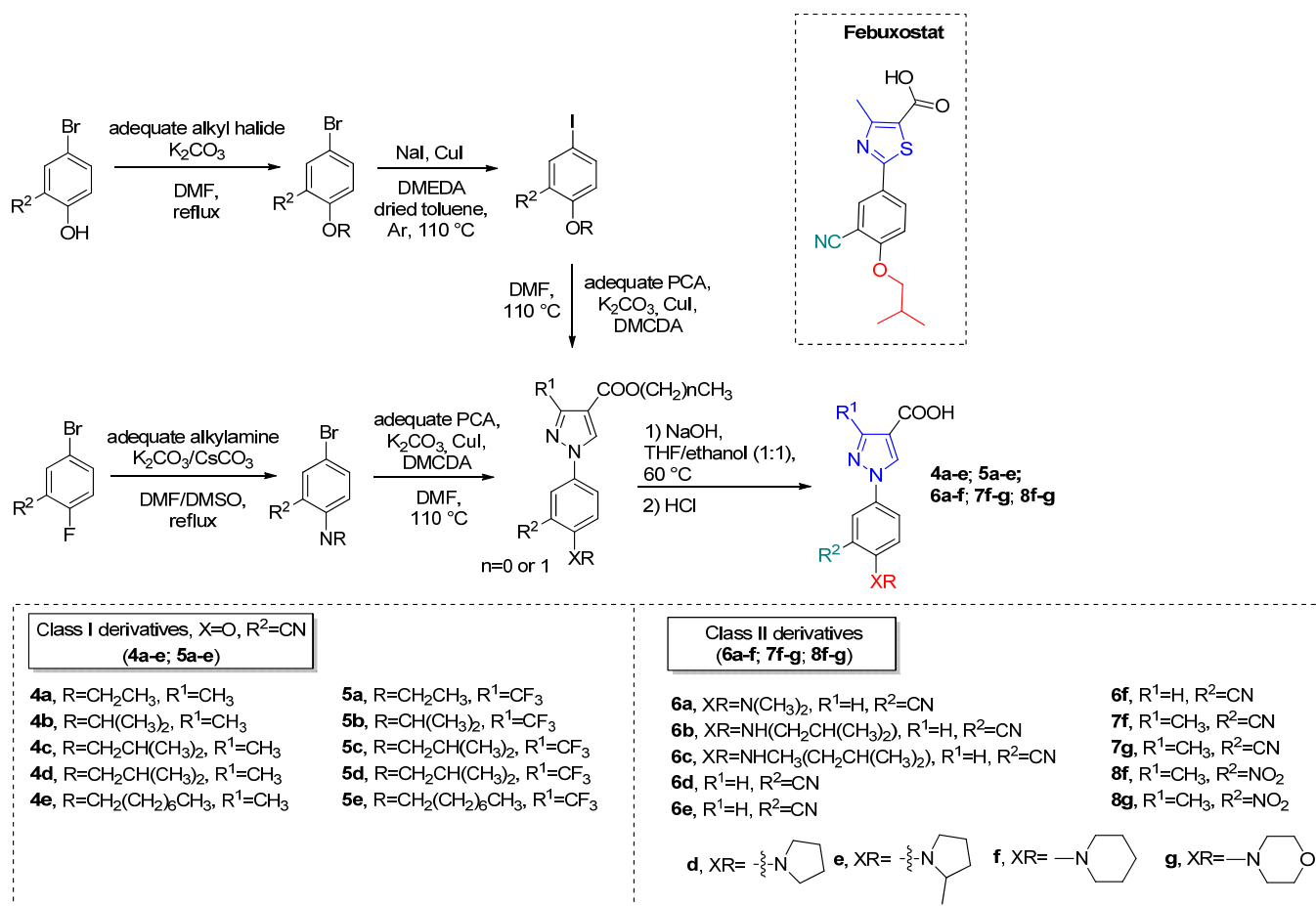
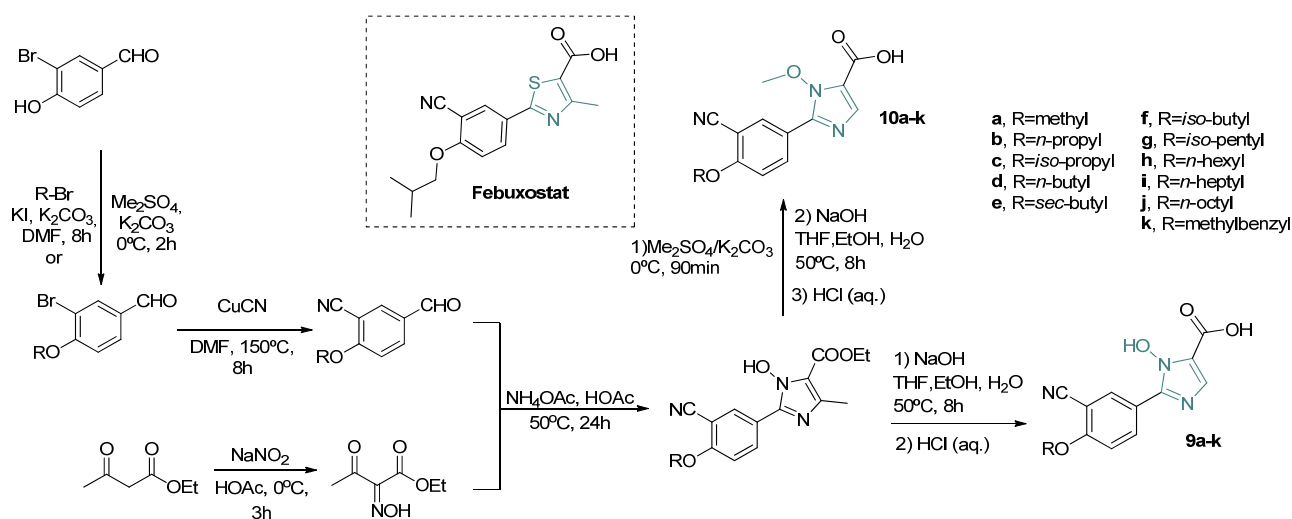
**Scheme 4.** Synthesis of 1-phenyl-pyrazole-4-carboxylic acids class I derivatives **4a–e**, **5a–e** and class II derivatives **6a–f**, **7f,g**, **8f,g** [40]. DMCDA = trans-N,N'-dimethyl-1,2-cyclohexane-diamine. PCA = 3-trifluoropyrazol-4-carboxylic acid or 3-methyl-4-carboxylic acid or *H*-pyrazol-4-carboxylic acid.

Table 2. 1-phenyl-pyrazole-4-carboxylic acids class I derivatives **4a–e**, **5a–e** and class II derivatives **6a–f**, **7f,g**, **8f,g** in vitro XO inhibition potential in terms of IC₅₀ [40].

Compound	IC ₅₀ (nM)	Compound	IC ₅₀ (nM)	Compound	IC ₅₀ (nM)
4a	>100	5d	>100	7f	13.3
4b	45	5e	>100	7g	>100
4c	n.t.	6a	10.8	8f	59.6
4d	23	6b	7.7	8g	>100
4e	>100	6c	5.7	Y-700	3.5
5a	>100	6d	5.7	Febuxostat	5.3
5b	>100	6e	6.7		
5c	>100	6f	4.2		

n.t. = not tested.

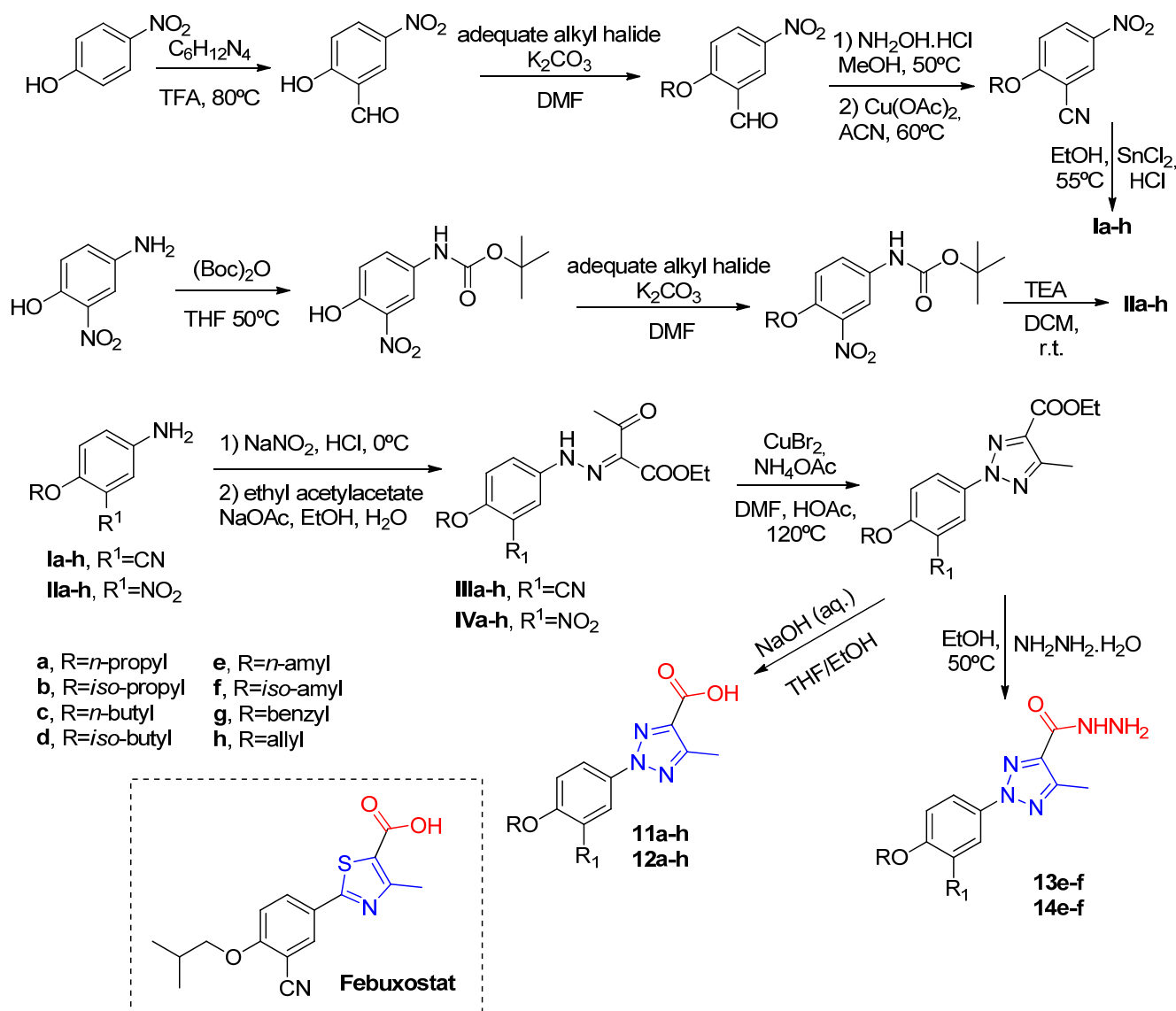
Another deviation in the five-member ring, proposed by Chen and coworkers [41], comprised the replacement of the thiazole group for the 1-hydroxy/methoxy-imidazole ring (Scheme 5). The in vitro IC₅₀ of XO inhibition of the hydroxy-imidazole (**9a–k**) class presented significantly lower values than the methoxy-imidazole class (**10a–k**) (Table 3). Improvement of the activity was found for intermediary carbon chain length substituents at the 4-position (*n*-butoxy, *sec*-butoxy, and *iso*-butoxy). Docking analysis of one of the most potent compounds tested (**9f**, in vitro IC₅₀ of 6 nM) showed that the hydroxyl group bonded to the nitrogen atom of the imidazole ring improved the interaction with the active site of XO through an additional hydrogen bond with Thr1010. Kinetic assays revealed that the compound **9f** inhibition mechanism for XO was a mixed type.

**Scheme 5.** 1-hydroxy (**9a–k**) and 1-methoxy (**10a–k**) 4-methyl-2-phenyl-1H-imidazole-5-carboxylic acid derivatives [41].**Table 3.** In vitro XO inhibitory potency of imidazole-5-carboxylic acid derivatives **9a–k**, **10a–k** [41].

Compound	IC ₅₀ (nM)	Compound	IC ₅₀ (nM)	Compound	IC ₅₀ (nM)
9a	550	9i	110	10f	n.a
9b	130	9j	1200	10g	8000
9c	170	9k	110	10h	3900
9d	3	10a	n.a	10i	n.a
9e	3	10b	n.a	10j	n.a
9f	6	10c	n.a	10k	1100
9g	30	10d	n.a	Febuxostat	10
9h	30	10e	1500		

n.a. = not active (<50% inhibition at 10 µg/mL).

Following the same strategy, Shi and coworkers [42] have synthesized two classes of compounds by replacing the thiazole ring of febuxostat with a 1,2,3-triazole ring containing a carboxylic acid (**11a–h**, **12a–h**) or a carbohydrazide substituent (**13e,f**, **14e,f**) (Scheme 6). Among the tested compounds, those with carboxyl moiety presented *in vitro* IC₅₀ values ranging between 84–254 nM, while those compounds with carbohydrazide substituents were not active for XO inhibition (Table 4). The most active compounds were those with *i*-amyl at the R-position, and cyano group or nitro group at R¹ (**11f**, *in vitro* IC₅₀ = 84 nM and **12f**, *in vitro* IC₅₀ = 109 nM). However, when compared to febuxostat (*in vitro* IC₅₀ = 12 nM), those compounds displayed a slight decrease in inhibition potential. A docking analysis reveals similar interactions found in febuxostat and, in addition, it was observed that the nitrogen atom at the 3-position of triazole forms a hydrogen bond with Glu802 and an additional π - π interaction of the five-member ring with Phe1009.



Scheme 6. 2-phenyl-5-methyl-2H-1,2,3-triazole-4-carboxylic acid (**11a–h**, **12a–h**) and carbohydrazide (**13e,f**, **14e,f**) derivatives [42].

Table 4. In vitro XO inhibitory potency 2-phenyl-5-methyl-2H-1,2,3-triazole-4-carboxylic acid (**11a–h**, **12a–h**) and carbohydrazide (**13e,f**, **14e,f**) derivatives [42].

Compound	IC ₅₀ (nM)	Compound	IC ₅₀ (nM)	Compound	IC ₅₀ (nM)
11a	195	11h	225	12g	180
11b	177	12a	162	12h	254
11c	135	12b	145	13e	n.a
11d	105	12c	151	13f	n.a
11e	112	12d	123	14e	n.a
11f	84	12e	125	14f	n.a
11g	152	12f	109	Febuxostat	12

n.a. = not active (<50% inhibition at 10 µg/mL).

Zhang and coworkers [43] have also synthesized, tested, and compared febuxostat analogs **15a–s** containing the 1,2,3-triazole nucleus as XO inhibitors (Scheme 7) to allopurinol, Y-700, and febuxostat as positive controls. However, in this case, the difference compared to the previously discussed Shi and coworkers' work [42] is in the isosteric replacement of the nitrogen atoms. The proximity of the X¹-position with molybdenum-pterin inspired the authors to replace a carbon atom at this position with a nitrogen atom. The majority of the tested compounds presented an in vitro IC₅₀ value lower than allopurinol (7.56 µM), but greater than Y-700 (0.016 µM) (Table 5). SAR analysis showed that the lipophilicity at the R may be beneficial for the activity. The increase of the carbon chain from three to eight at the R leads to a significant increase in XO inhibition potential (IC₅₀ > 30 µM to IC₅₀ = 0.63 µM). An improvement of inhibition activity was also achieved by insertion of benzyl groups as R, as the *meta*-Methoxybenzyl group (**15s**) presented the lower in vitro IC₅₀ value of 0.21 µM. Docking analysis showed a similar interaction compared to febuxostat and the active site of XO, including the triazole ring aromatic interaction with Phe1009 and Phe914. However, the nitrogen atom at X²-position does not seem to have any interaction with molybdenum-pterin as expected. Moreover, neighboring X²-position nitrogen seemed to increase the hydrophilicity around the X¹-position nitrogen, leading to the observed decrease in derivatives potency.

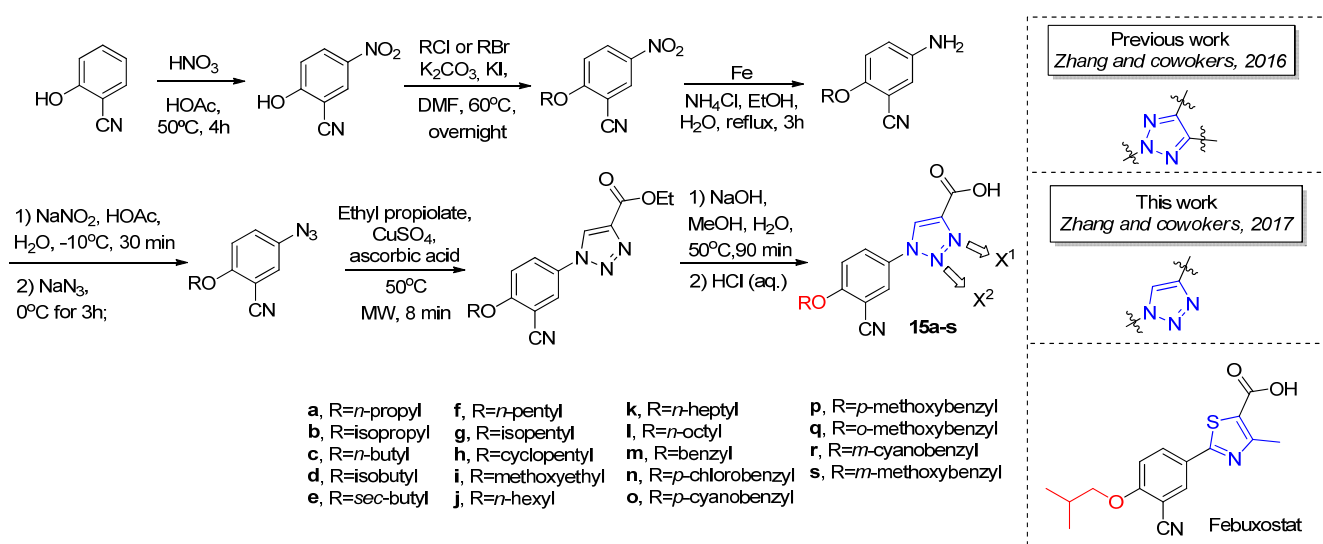
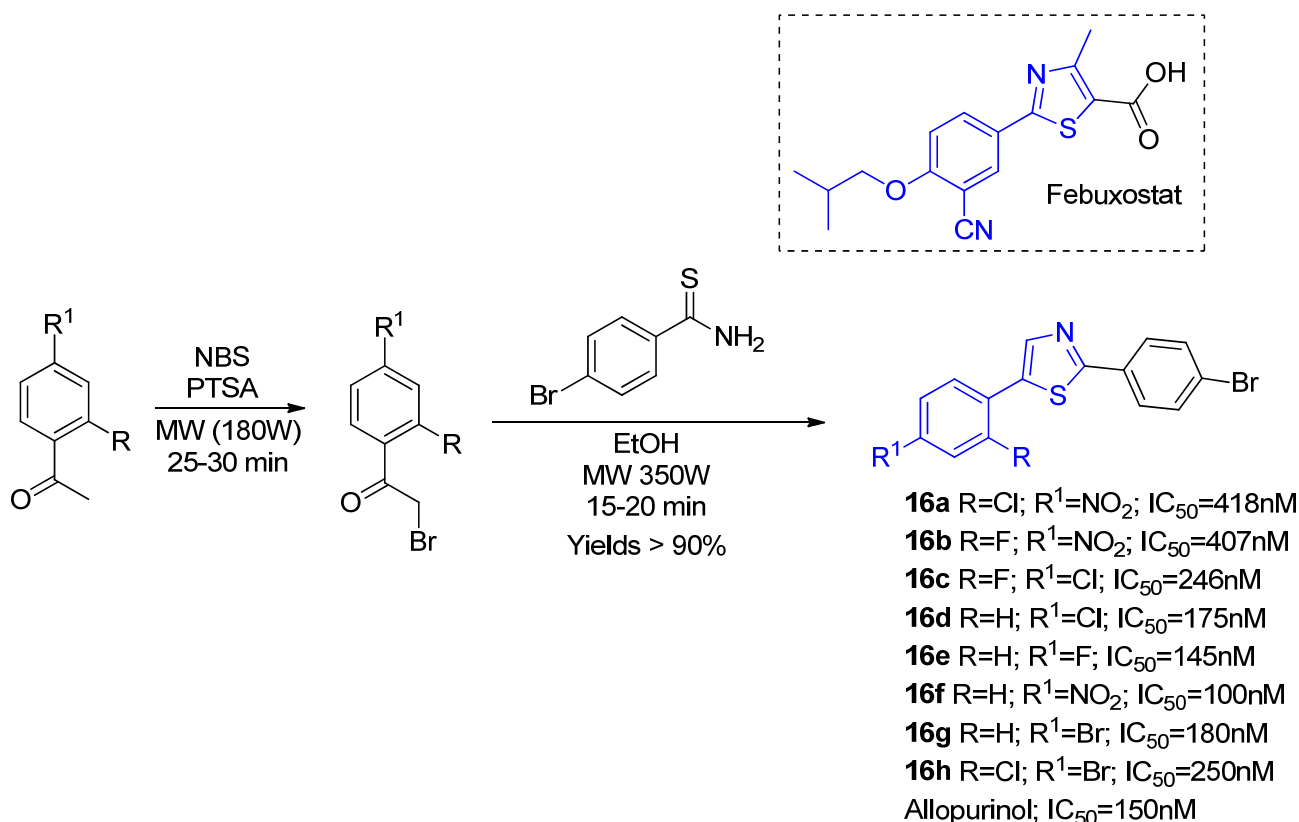
**Scheme 7.** 1-phenyl-1H-1,2,3-triazole-4-carboxylic acid derivatives **15a–s** [43].

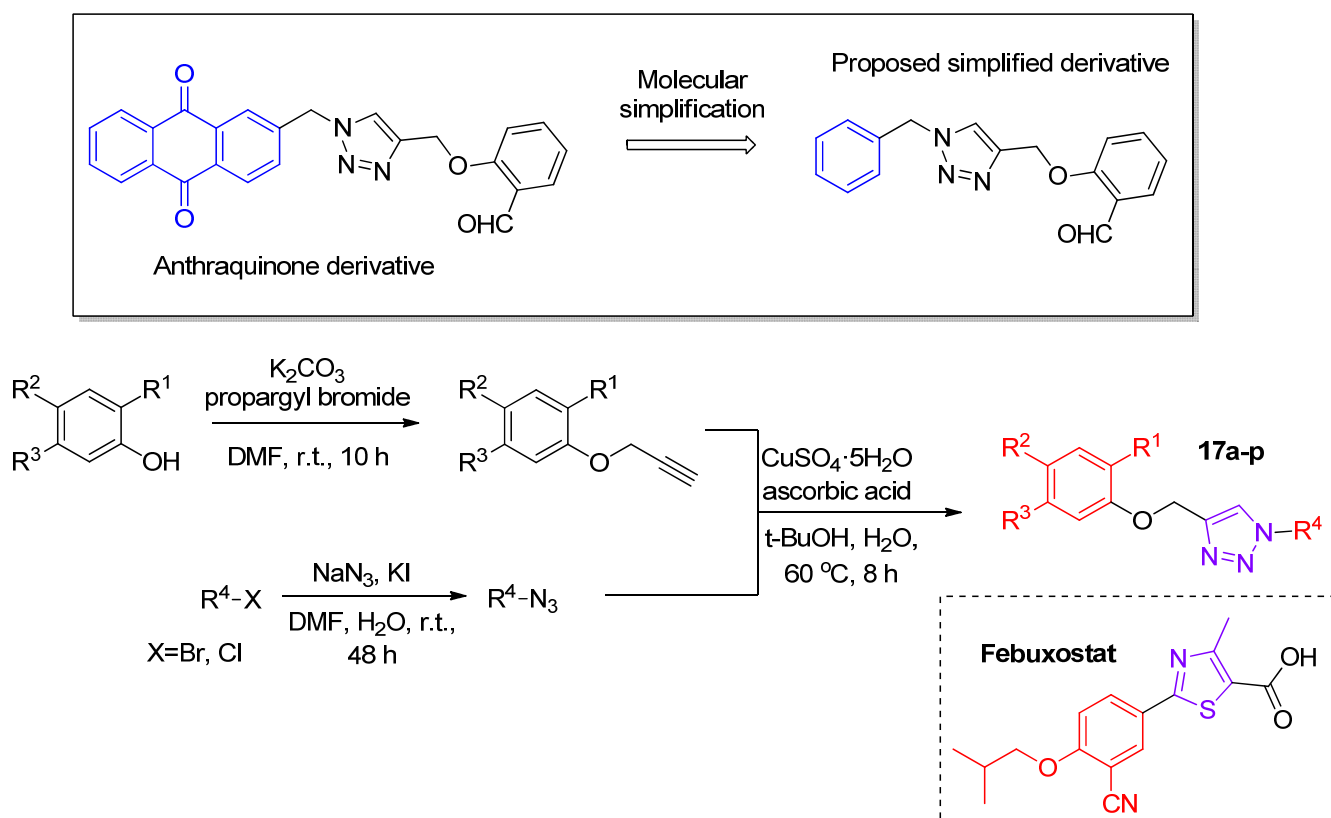
Table 5. In vitro XO inhibitory potency of 1-phenyl-1*H*-1,2,3-triazole-4-carboxylic acid derivatives **15a–s** in terms of IC₅₀ [43].

Compound	IC ₅₀ (μM)	Compound	IC ₅₀ (μM)	Compound	IC ₅₀ (μM)
15a	>30	15h	1.08	15o	0.85
15b	6.24	15i	26.13	15p	0.72
15c	5.03	15j	1.50	15q	0.76
15d	3.27	15k	1.47	15r	3.35
15e	3.96	15l	0.63	15s	0.21
15f	2.85	15m	2.40	Allopurinol	7.56
15g	1.62	15n	0.94	Y-700	0.016

Exploring a microwave-assisted synthetic strategy, Jyothi and coworkers [44] produced eight novel XO inhibitors (**16a–h**) comprising febuxostat's thiazole nucleus through a highly efficient two-step procedure (Scheme 8). The group had also tested the same reaction conditions under thermal heating, in which case the reactions needed between three to five hours and the yields dropped to 64–76%. All the synthesized compounds presented in vitro XO inhibition activities in the nanomolar range. However, the derivatives **16e,f** showed the greatest potency, with lower IC₅₀ values (IC₅₀ = 145 nM and 100 nM, respectively) than the control drug allopurinol (IC₅₀ = 150 nM). A SAR investigation pointed out that electron withdrawing groups at the phenyl ring *para* position are beneficial for the inhibitory activity improvement. Molecular docking with the most active compound **16f** pointed out a stronger binding affinity (−9.1 kcal/mol) compared to allopurinol (−7.0 kcal/mol) and more non-binding interaction with amino acids residues within the XO active site, which lead to a more stable bond with the enzyme. A molecular dynamic assay pointed out that there were no significant structural changes from the docked model.

**Scheme 8.** Synthetic procedure employing microwave to obtain the novel phenyl thiazole derivatives **16a–h** and its XO inhibitory activities in terms of in vitro IC₅₀ [44].

Based in the molecular skeleton of an anthraquinone derivative previously synthesized by the group, which presented a promising XO inhibition activity of 0.61 mM, Zhang and coworkers [45] developed novel XO inhibitors. Two of the group's major concerns regarding the anthraquinone based derivative were the high lipophilicity giving a poor drug-like characteristic and the DNA binding affinity leading to potential collateral cytotoxic effects. Thus, molecular deviations were proposed, and more than thirty-five compounds were obtained. We present the most active ones and some analogues **17a–p** to discuss important SAR characteristics (Scheme 9). The best IC_{50} values were achieved with either the introduction of a fluorine atom at the benzaldehyde R^2 position and/or a *meta*-methoxybenzyl at R^4 position (Table 6). The absence of aldehyde functionalization at R^1 position resulted in inactive compounds for the chosen criteria of 25 μ M maximum concentration for the *in vitro* activity assays. Moreover, docking analysis showed hydrophobic interactions of the *meta*-methoxybenzyl with Phe649 and Phe1013 and a well-adjusted accommodation of the *meta*-fluorine benzaldehyde moiety at the hydrophobic pocket of XO composed of Leu873, Ala1078, and Val1011 amino acids, justifying the promising results comprising those deviations. The parameters metrics of ligand efficiency (LE) and lipophilic ligand efficiency (LLE) were employed to correlate biological activity with the lipophilicity of the most potent compounds showing an important improvement of those parameters with respect to allopurinol used as a positive control, including high solubility in the buffer. Additionally, *in vivo* tests with the most potent compound **17h** showed a 31% of serum uric acid levels reduction in vehicle-treated rats at a dose of 20 mg/kg after 2 h compared to the control, which highlights the selected compound as a promising lead compound.



Scheme 9. Selected 1,2,3-triazole derivatives **17a–p** synthesis protocol [45].

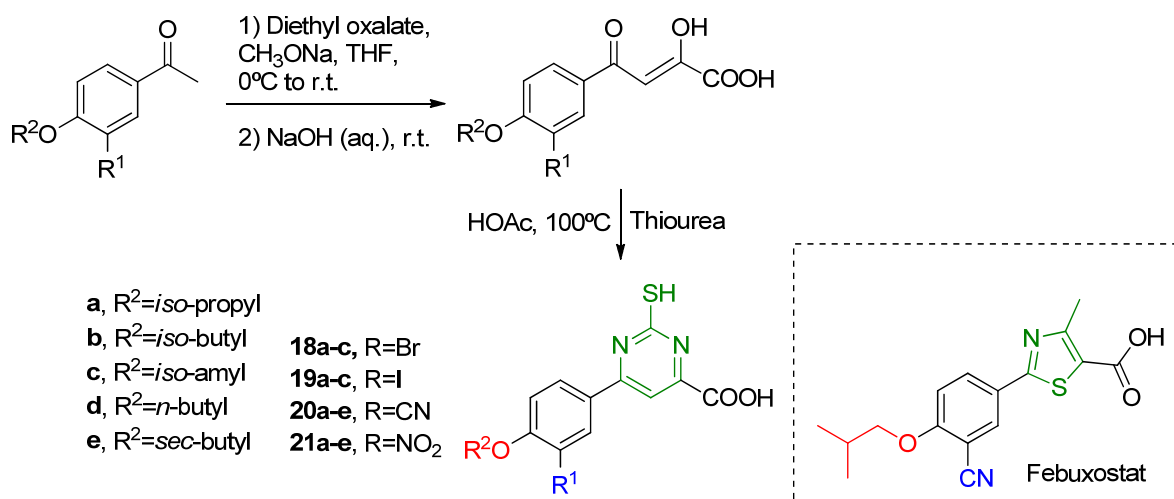
Table 6. Selected 1,2,3-triazole derivatives **17a–p** and its in vitro XO inhibitory activity in terms of IC₅₀ [45].

Compound	R ¹	R ²	R ³	R ⁴	IC ₅₀ (μM)
8d(17a)	CHO	H	H	<i>n</i> -butyl	13.50
8h(17b)	CHO	H	H	<i>iso</i> -pentyl	16.03
8l(17c)	CHO	H	H	<i>o</i> -methoxybenzyl	1.45
8m(17d)	CHO	H	H	<i>m</i> -methoxybenzyl	1.02
9d(17e)	CHO	F	H	<i>n</i> -butyl	2.49
9h(17f)	CHO	F	H	<i>iso</i> -pentyl	2.12
9l(17g)	CHO	F	H	<i>o</i> -methoxybenzyl	0.94
9m(17h)	CHO	F	H	<i>m</i> -methoxybenzyl	0.70
10d(17i)	CHO	H	F	<i>n</i> -butyl	3.59
10h(17j)	CHO	H	F	<i>iso</i> -pentyl	n.a.
10l(17k)	CHO	H	F	<i>o</i> -methoxybenzyl	2.07
10m(17l)	CHO	H	F	<i>m</i> -methoxybenzyl	n.a.
13l(17m)	CN	H	H	<i>o</i> -methoxybenzyl	n.a.
13m(17n)	CN	H	H	<i>m</i> -methoxybenzyl	n.a.
14l(17o)	NO ₂	H	H	<i>o</i> -methoxybenzyl	n.a.
14m(17p)	NO ₂	H	H	<i>m</i> -methoxybenzyl	n.a.
Allopurinol	-	-	-	-	9.80

n.a. = not active (<50% inhibition at 25 μM).

3.1.2. Derivatives Based on Six-Member Heterocyclic Rings

Febuxostat analogs have also been explored with a six-member heterocycle instead of the five-member. This is the case of 2-mercapto-6-phenylpyrimidine-4-carboxylic acid derivatives **18a–c**, **19a–c**, **20a–e**, **21a–e** synthesized by Shi and coworkers (Scheme 10) [26]. The thiazole ring was replaced by a mercapto-pyrimidine moiety, and the inhibition activity was compared to febuxostat (Table 7). It was observed that the most promising compound (**20b**) had a cyano group at R¹ and an *iso*-butyl substituent at R², presenting an in vitro IC₅₀ of 132 nM. However, the inhibition potency was approximately ten times lower than febuxostat (in vitro IC₅₀ = 13 nM). The other derivatives retained the nanomolar potency, but presented even higher in vitro IC₅₀ values. SAR showed that the cyano group is more promising than other electron-withdrawing substituents such as nitro, iodine, and bromide. However, as foreseen by molecular docking, changes in the structure show that the cyano group from phenyl moiety does not properly interact with the XO active site, whereas the mercapto group interacts via a hydrogen bond with Mos4004 and protonated Glu802 residue. Kinetic assays revealed the mixed type inhibition mechanism of **20b**, similar to febuxostat and Y-700.



Scheme 10. 2-mercapto-6-phenylpyrimidine-4-carboxylic acid derivatives **18a–c**, **19a–c**, **20a–e**, **21a–e** [26].

Table 7. In vitro XO inhibitory potency of 2-mercapto-6-phenylpyrimidine-4-carboxylic acid derivatives. **18a–c**, **19a–c**, **20a–e**, **21a–e** in terms of IC₅₀ [26].

Compound	IC ₅₀ (nM)	Compound	IC ₅₀ (nM)	Compound	IC ₅₀ (nM)
18a	674	19e	417	21b	283
18b	798	20a	208	21c	510
18c	1.13	20b	132	21d	421
19a	322	20c	282	21e	333
19b	463	20d	377	Febuxostat	13
19c	527	20e	138		
19d	471	21a	292		

Using a similar strategy, Zhang and coworkers [46] synthesized two classes of pyridazine derivatives by replacement of the thiazole group of febuxostat with a six-member heterocycle moiety. The first two steps of the strategic synthesis were similar for both classes of compounds. The procedure followed the hydrazinolysis pathway to obtain the carbohydrazide derivatives **22a–o** or the hydrolysis pathway to obtain the carboxylic acid derivatives **23c,d,h** (Scheme 11). Surprisingly, the carboxylic acid derivatives **23c,d,h** were not active, while the carbohydrazide derivatives **22a–o** presented lower in vitro IC₅₀ than allopurinol (in vitro IC₅₀ = 6.43 μM), but much higher than febuxostat (in vitro IC₅₀ = 0.018 μM) (Table 8). The difference in the two classes of compounds activity was explained through molecular docking analysis of analog structures, 6-(3-Cyano-4-isobutoxyphenyl)-3-oxo-2,3-dihydropyridazine-4-carbohydrazide (**22c**) and 6-(3-Cyano-4-isobutoxyphenyl)-3-oxo-2,3-dihydropyridazine-4-carboxylic acid (**23c**). According to this analysis, more prominent interactions were found between the carbohydrazide group with the XO active site than a carboxylic acid. The carbohydrazide group of **23c** forms hydrogens bonds with Ag880, Glu802, and Mos3004 residues, while the carboxylic acid of **22c** only interacts with Glu802. SAR analysis related to the R¹ and R² phenyl substituents showed that both cyano and nitro groups at R¹ with O-iso-propyl at R² are beneficial for inhibition activity (IC₅₀ of 1.03 μM and 1.92 μM, for **22b** and **22h**, respectively). Kinetic studies comprising the most potent compound (**22b**) pointed out a mixed-type inhibition mechanism.

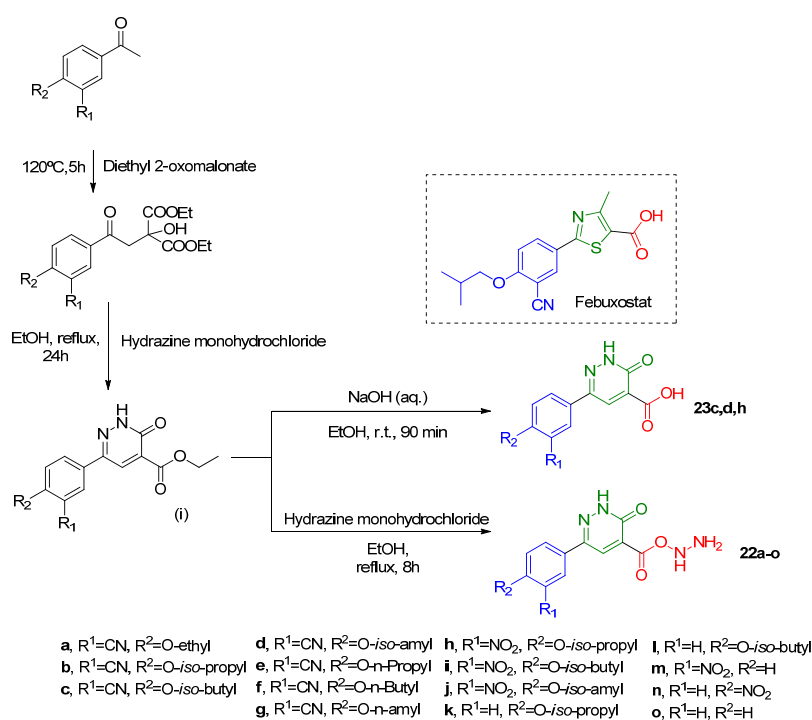
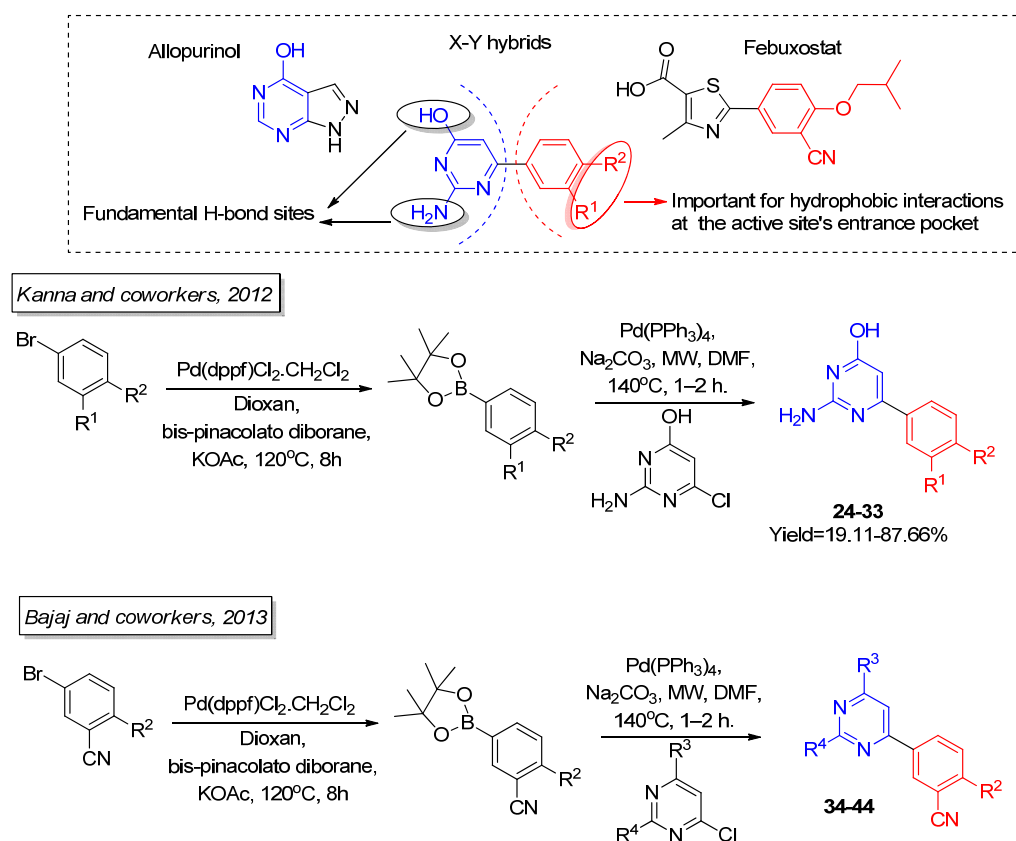
**Scheme 11.** Six-membered heterocycles pyridazine derivatives **22a–o**, carboxylic acid derivatives **23c,d,h** [46].

Table 8. In vitro XO inhibitory potency of six-membered heterocycles pyridazine derivatives **22a–o**, carboxylic acid derivatives **23c,d,h** and their in vitro XO inhibition potential in terms of IC_{50} [46].

Compound	IC_{50} (μ M)	Compound	IC_{50} (μ M)	Compound	IC_{50} (μ M)
22a	2.54	22h	1.92	23c	n.a.
22b	1.03	22i	3.65	23d	n.a.
22c	2.97	22j	6.02	23h	n.a.
22d	4.50	22k	n.a.	Allopurinol	6.43
22e	3.10	22m	n.a.	Febuxostat	0.018
22f	5.24	22n	n.a.		
22g	5.89	22o	n.a.		

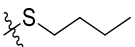
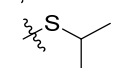
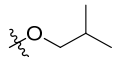
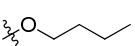
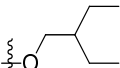
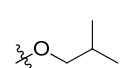
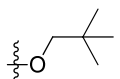
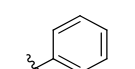
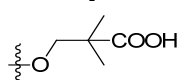
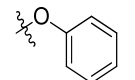
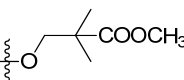
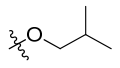
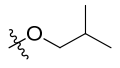
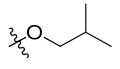
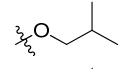
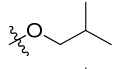
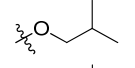
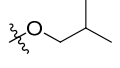
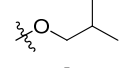
n.a. = not active (<50% inhibition at 10 μ g/mL).

Guided by SAR studies, Khanna and coworkers managed to successfully plan diverse structural modification in the isocytosine scaffold [47], which was further explored by the same research group by synthesizing and testing novel molecular deviations [48]. Isocytosine was earlier recognized as a promising lead compound to be explored as a XO inhibitor by the group's virtual screening collection. More than thirty novel allopurinol and febuxostat hybrid compounds, of which we highlight the most promising ones, **24–32** and **33–43** (Scheme 12), were organized by structural similarity to detach the SAR influence in modulating the biological activity (Table 9), with extremely low values of in vitro IC_{50} compared to the control drugs allopurinol and febuxostat. Moreover, **29**, **30**, **32**, and **43** presented good in vivo efficacy in a hyperuricemic rat model compared to allopurinol. The conjugation of allopurinol and febuxostat molecular fractions might explain the promising results consisting of lead compounds where the $-NH_2$ and $-OH$ groups of isocytosine formed fundamental hydrogen bonds with the target's active site in limited SAR studies, while the R^1 and R^2 substituents played a key role by managing hydrophobic interactions at the active site pocket's entrance by both electrostatic interactions and steric effects.



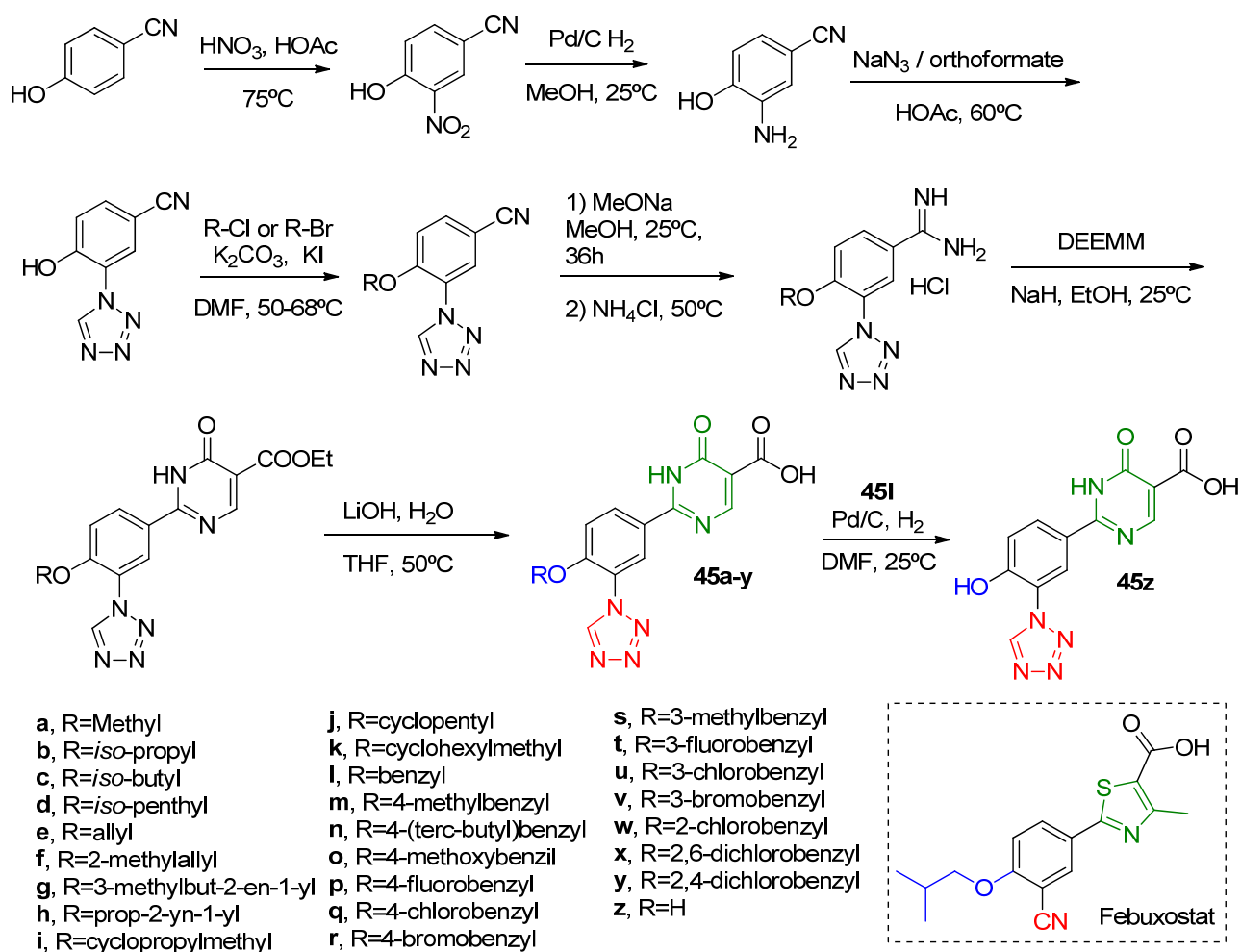
Scheme 12. Synthesis of the isocytosine derivatives **22–31** and **32–42** as XO inhibitors [47,48].

Table 9. Derivatives 24–33 and 34–44 in vitro XO inhibition activity in terms of IC₅₀.

Derivative ^a	R ¹	R ²	IC ₅₀ (μM)	Derivative ^b	R ²	R ³	R ⁴	IC ₅₀ (μM)
24	H		1.63	34	OCH ₃	OH	NH ₂	0.160
25	H		2.44	35		OH	NH ₂	0.018
26	H		2.10	36		OH	NH ₂	0.010
27	H		0.60	37		OH	NH ₂	0.004
				Allopurinol	-	-	-	4.500
				Febuxostat	-	-	-	0.020
32	H		0.31	38		OH	NH ₂	0.005
33	H		2.47	39		OH	NH ₂	0.015
Allopurinol	-	-	4.19	40		COOH	NH ₂	0.400
Febuxostat	-	-	0.03	41		CONH ₂	NH ₂	3.900
28	-	-	1.92	42		OH	H	0.060
29	OCH ₃		0.95	43		OH	CH ₃	>30
30	NO ₂		0.14	44		H	NH ₂	0.080
31	CN		0.02	Allopurinol	-	-	-	4.200
Allopurinol	-	-	5.77	Febuxostat	-	-	-	0.020
Febuxostat	-	-	0.03					

Reference compounds allopurinol and febuxostat appear right below the corresponding assay derivatives; ^a [47]; ^b [48].

A multi-step synthesis of febuxostat–allopurinol hybrids **45a–z** (Scheme 13) was made by Zhang and coworkers [49] to explore the isosteric replacement of the cyano group of the above-discussed works molecules [47,48] and execute a SAR analysis. XO inhibition was evaluated through IC₅₀ analysis that, in general, had values comparable to febuxostat (Table 10). The most active compounds had *meta*-chlorobenzyl or *meta*-bromobenzyl anchored at R with in vitro IC₅₀ of 28.8 nM (**45u**) and 45.0 nM (**45v**). A SAR analysis showed that hydrophobic compounds at R are essential for a good inhibition potential. Docking studies of the most potent inhibitor (**45u**) showed that the tetrazole ring can be accommodated at the XO active site and form hydrogen bonds with Asn768 and Lys771; additionally, the carboxyl group of pyrimidine also interacts with Ag880 and Mo-OH residues. The six-membered heterocycle group of **45u** shows the same aromatic interactions as the thiazole group in febuxostat, while chlorobenzyl displays a π–π interaction with Phe649. Lastly, in vivo analysis demonstrated that oral administration of a single dose (5 mg/kg) of **45u** in hyperuricemic rats, by administration of potassium oxonate, can lower the serum levels of UA.



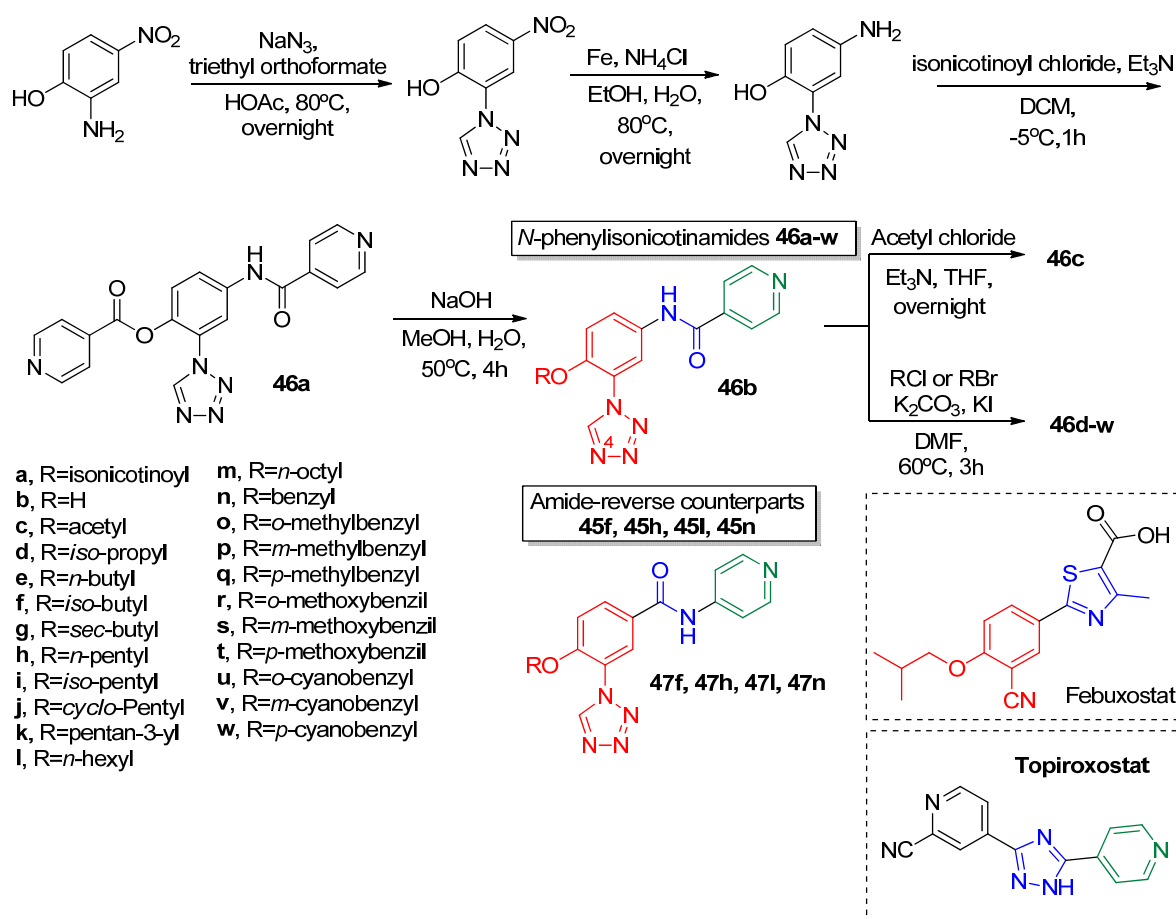
Scheme 13. Febusostat derivatives 45a–z containing a tetrazole nucleus as replacement of the original cyano group [49]. DEEMM = Diethyl ethoxymethylenemalonate.

Table 10. Febusostat derivatives 45a–z and its in vitro XO inhibition potential in terms of IC₅₀ [49].

Compound	IC ₅₀ (nM)	Compound	IC ₅₀ (nM)	Compound	IC ₅₀ (nM)
45a	92.0	45j	58.5	45s	51.6
45b	73.7	45k	68.3	45t	47.7
45c	64.4	45l	94.5	45u	28.8
45d	54.1	45m	89.4	45v	45.0
45e	43.7	45n	149	45w	91.7
45f	56.9	45o	50.7	45x	63.9
45g	69.2	45p	53.1	45y	83.8
45h	50.0	45q	69.1	45z	629
45i	46.1	45r	55.2	Febusostat	23.6

A complementary work by Zhang and coworkers further explored the bioisosteric replacement of the febusostat cyano group by the 1,2,3,4-tetrazole [50]. The synthesized derivative 46a–w (Scheme 14) hybrids based in topiroxostat and febusostat molecular scaffold presented potency in the nanomolar range (IC₅₀ between 31 nM and 603 nM), except for 46a–b, which were inactive (Table 11). The general R group influence trend over activity modulation was that increasing hydrophobicity and volume led to better XO inhibition. Additionally, aromatic groups containing electron-withdrawing components at a meta position (46s and 46v) seemed to be the most beneficial pattern to obtain high potency derivatives. Moreover, they further synthesized the analogs 47f,h,l,n. Differently

from **46a–w**, where the cyanophenyl portion was bonded to the nitrogen atom of the amide linker, the N-phenylisonicotinamide counterparts **47f,h,l,n** ended up being over twenty times less active (Table 11). A molecular docking study and a molecular dynamics simulation for the most active hybrid **46v** revealed a strong interaction with the XO's active site as tetrazole N⁴ nitrogen and Asn768; pyridine *para*-N and Glu1261; cyano group and Ser876 (two H-bonds at the same time, one by the amino acid OH group and the other by NH group); and carbonyl group with Arg880 and Thr1010 via a water bridge. Lastly, kinetic studies involving the selected hybrid **46v** revealed a mixed-type of inhibition mechanism.



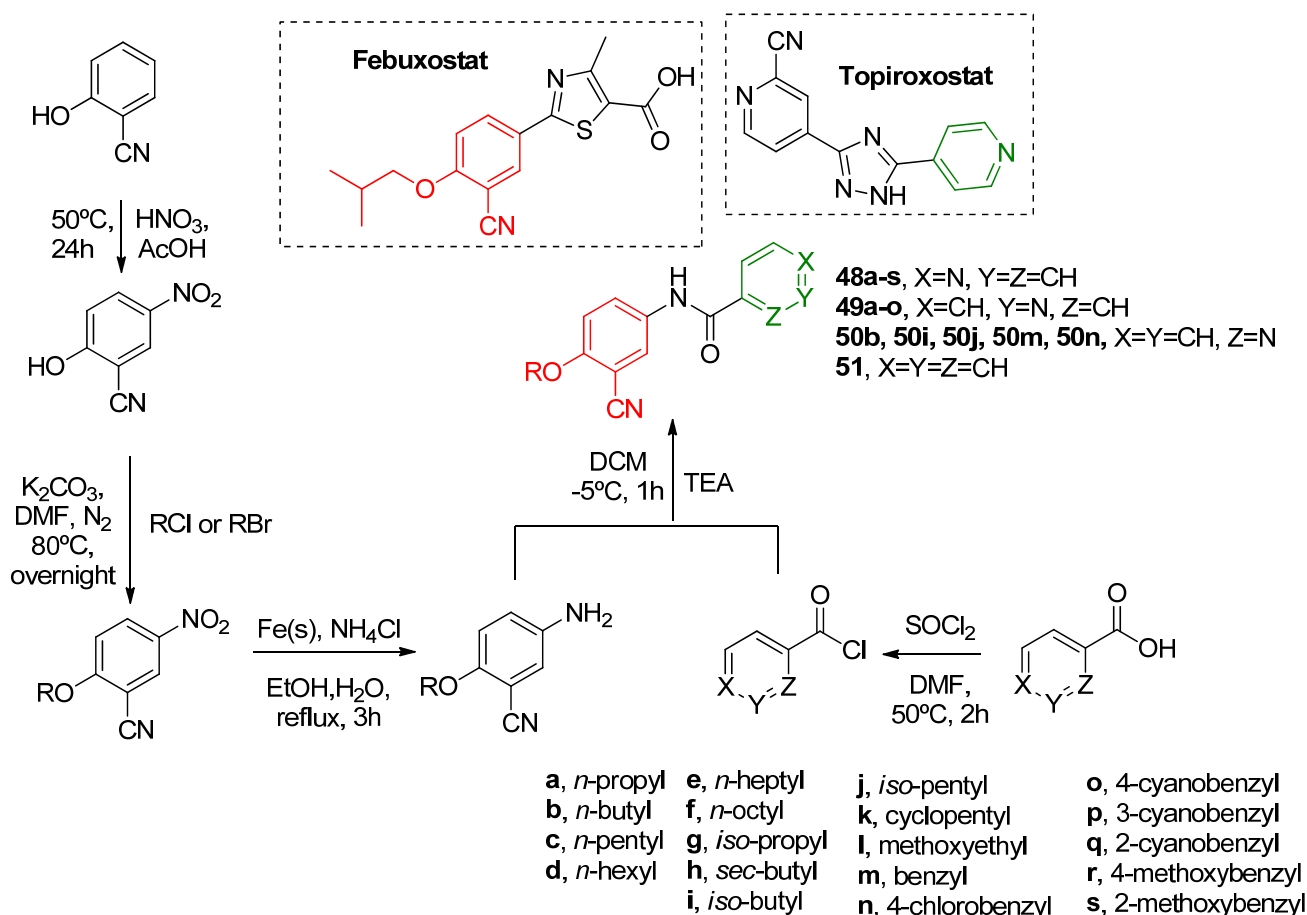
Scheme 14. Synthesis of derivatives **46a–w** and its amide-reverse counterparts **47f,h,l,n** (synthesis not shown) comprising the bioisosteric replacement of the febugostat cyano group by the 1,2,3,4-tetrazole [50].

Table 11. In vitro XO inhibition potential in terms of IC₅₀ of derivatives **46a–w** and **47f,h,l,n** comprising the bioisosteric replacement of the febugostat cyano group by the 1,2,3,4-tetrazole [50].

Compound	IC ₅₀ (nM)	Compound	IC ₅₀ (nM)	Compound	IC ₅₀ (nM)
46a	n.a.	46k	141	46u	110
46b	n.a.	46l	153	46v	31
46c	173	46m	92	46w	100
46d	603	46n	94	47f	2890
46e	264	46o	53	47h	3860
46f	165	46p	44	47l	4590
46g	171	46q	132	47n	2100
46h	174	46r	117	Topiroxostat	21
46i	145	46s	50		
46j	128	46t	67		

n.a. = not active (<60% inhibition at 10 μM).

Motivated to obtain different hybrid derivatives based in topiroxostat and febuxostat molecular structures, Zhang and coworkers [51] explored hybrid structures of isonicotinamide (**48a–s**), nicotinamide (**49a–o**), picolinamide (**50b,i,j,m,n**), and benzamide (**51**) derivatives where the pyridine moiety nitrogen position also varied (Scheme 15). This time using an amide linker as an isosteric replacement for the previously discussed imidazole linker. SAR showed that large linear carbon chains lead to reduced potency derivatives (Table 12), as observed by the increase in IC_{50} values from **48b** (in vitro $IC_{50} = 2.3 \mu\text{M}$) to **48f** (in vitro $IC_{50} = 19.2 \mu\text{M}$). Additionally, *ortho*- (**49a–o**), *meta*-N (**50b,i,j,m,n**) and N absence (**51**) lead mostly to unactive derivatives. On the other hand, aromatic R groups in *para*-N derivatives furnished some of the most potent inhibitors, such as **48q** with in vitro IC_{50} of $0.3 \mu\text{M}$ and **48r** with in vitro IC_{50} of $0.6 \mu\text{M}$. Overall, sixteen out of the nineteen isonicotinamide derivatives were more potent than allopurinol (in vitro $IC_{50} = 8.5 \mu\text{M}$), but less active than febuxostat (in vitro $IC_{50} = 0.015 \mu\text{M}$). As observed through molecular docking studies, isonicotinamide *para*-N formed a fundamental H-bond with Glu1261 residue. Moreover, regarding the amide group, pronounced interactions with Thr1010, Arg880, and Glu802 were observed, distancing the cyano group from Asn768, which probably lead to the decreased potency of isonicotinamide derivatives compared to febuxostat and its analogs. Lastly, kinetic studies revealed **48q** as a mixed-type inhibitor of XO. Which might be explained by potent inhibition of oxidized and reduced forms of XO.



Scheme 15. Isonicotinamide (**48a–s**), nicotinamide (**49a–o**), picolinamide (**50b,i,j,m,n**) and benzamide (**51**) derivatives [51].

Table 12. Isonicotinamide (48a–s), nicotinamide (49a–o), picolinamide (50b,i,j,m,n), benzamide (51) derivatives and their in vitro XO inhibition potential in terms of IC₅₀ [51].

Compound	IC ₅₀ (μM)	Compound	IC ₅₀ (μM)	Compound	IC ₅₀ (μM)
48a	3.9	48k	5.7	49j	35.0
48b	2.3	48l	n.a.	49k	n.a.
48c	3.0	48m	0.9	49l	n.a.
48d	2.7	48n	0.8	49m	32.8
48e	5.0	48o	2.3	49n	n.a.
48f	19.2	48p	2.0	49o	n.a.
48g	9.5	48q	0.3	50b	n.a.
48h	6.1	48r	0.6	50i	n.a.
48i	1.6	48s	1.8	50j	n.a.
48j	2.0	49a-i	n.a.	50m	22.6
Allopurinol	8.5	Topiroxostat	0.015	50n	n.a.
				51	n.a.

n.a. = not active (<60% inhibition at 50 μM).

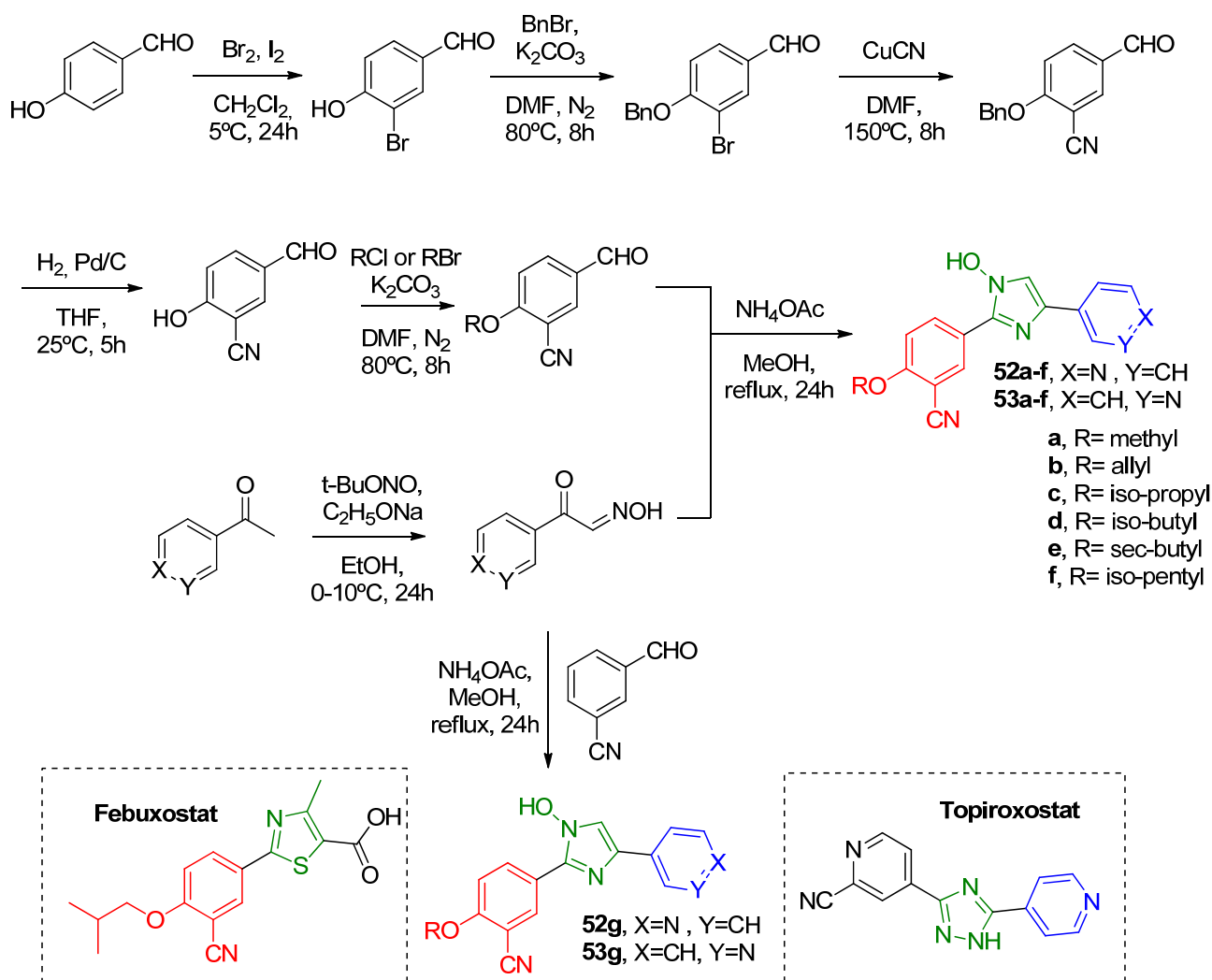
Under a similar approach, Zhang and coworkers [52] developed two novel families of isosteric compounds comprising a cyanophenyl-imidazole scaffold differently connected to a pyridine ring (Scheme 16). The novel synthesized topiroxostat-based *para*-substituted pyridine (52a–g) and *meta*-substituted pyridine (53a–g) also had an R sidechain varied with different hydrocarbon substituents for SAR investigation (Table 13). A SAR analysis pointed out that the steric effect of bulkier substituents contributed to better activity. Further, a 3D-QSAR model with the Topomer comparative molecular field analysis method was used to understand the interactions between 52f/53f and the XO active site. It was observed that pyridine with *para*-N forms a hydrogen bond with Glu1261 residue, while *meta*-N does not show any interaction, which could explain the great activity modulation between the isosteric compound families. Considering the aforementioned, the more pronounced activity of compound 52f (in vitro IC₅₀ = 0.64 μM) could be understood. However, it was still not as active as topiroxostat (in vitro IC₅₀ = 0.0048 μM). Lastly, kinetic studies involving 52f showed its mixed-type inhibition mechanism on XO.

Table 13. Topiroxostat-based isomeric family of derivatives 52a–g and 53a–g and its in vitro XO inhibition potential in terms of IC₅₀ [52].

Compound	IC ₅₀ (μM)	Compound	IC ₅₀ (μM)	Compound	IC ₅₀ (μM)
52a	15.42	52f	0.64	53d	10.28
52b	n.a.	52g	n.a.	53e	n.a.
52c	4.75	53a	n.a.	53f	6.73
52d	n.a.	53b	9.62	53g	n.a.
52e	4.35	53c	n.a.	Topiroxostat	0.0048

n.a. = not active (<60% inhibition at 10 μM).

Aiming an isosteric replacement of the amide linker by an 1,2,3-triazole nucleus, Zhang and coworkers [53] synthesized the novel febuxostat–topiroxostat hybrid derivatives 54a–p (Scheme 17) correlated with Zhang and coworkers' previous work [50]. These compounds presented a similar inhibition of XO to allopurinol, but lower than febuxostat (Table 14). The most potent compounds were those with *iso*-pentyl (54j) and cyclopentyl (54k) tails as substituents with IC₅₀ of 8.1 μM and 6.7 μM, respectively. Docking analysis of 54k reveals similar interactions of topiroxostat at the XO active site, including a lipophilic interaction of the cyclopentyloxy ether tail with Leu648, Phen649, and Phen1013 residues. Was also observed that substitution of the N atom at X²-position for a -CH was not favorable due to the distance increase of the triazole ring from the Glu802 residue.

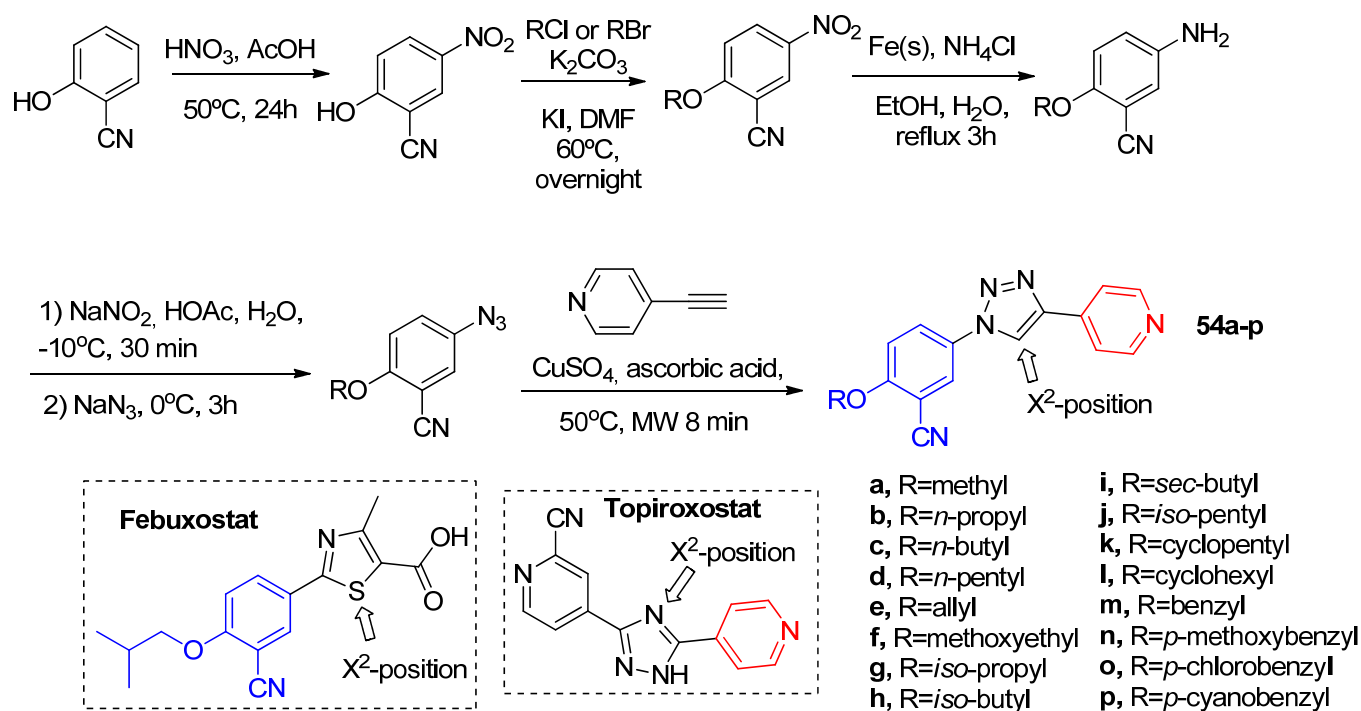


Scheme 16. Topiroxostat-based isomeric family of derivatives 52a–g and 53a–g [52].

Table 14. Febuxostat-topiroxostat hybrid derivatives 54a–p and their in vitro XO inhibition potential in terms of IC₅₀ [53].

Compound	IC ₅₀ (μM)	Compound	IC ₅₀ (μM)
54a	n.a.	54i	18.0
54b	n.a.	54j	8.1
54c	20.8	54k	6.7
54d	16.3	54l	n.a.
54e	n.a.	54m	45.0
54f	n.a.	54n	23.7
54g	25.4	54o	n.a.
54h	n.a.	54p	n.a.
Allopurinol	8.5	Topiroxostat	0.016

n.a. = not active (<50% inhibition at 50 μM).



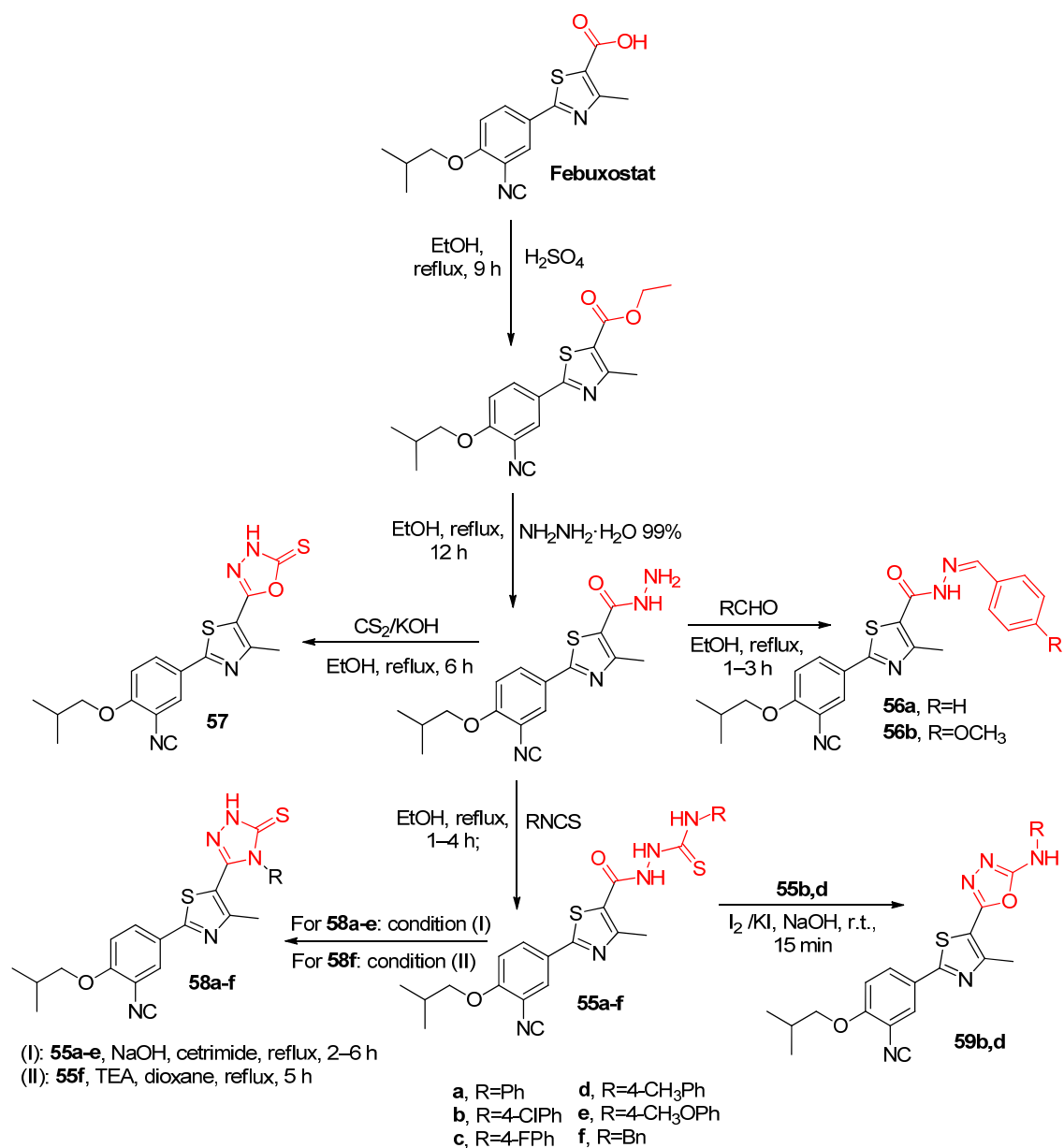
Scheme 17. Synthesis of the novel febusostat-topiroxostat hybrid derivatives **54a–p** with an isosteric replacement of the amide linker by an 1,2,3-triazole nucleus [53].

3.2. Bifunctionality: Two Challenges One Solution

3.2.1. XO Inhibition and Inflammatory Control in a Single Moiety

Recently, an extensive work was made by Rashad and coworkers [54] regarding the obtainment of febusostat derivatives comprising the carboxylic acid termination substitution into several functions like carboxamides, carbohydrazides, carbothioamides, benzonitriles, sulfonohydrazide and varied heterocyclics. The work required over twenty independent synthetic procedures and produced almost thirty novel derivatives. The authors aimed to obtain potent XO inhibitors that also detained relevant anti-inflammatory activity. This way, applicability for acute gout clinical conditions where joint inflammation is a challenging condition could be achieved.

Here, we highlight the obtainment of the five most promising compounds families, **55a–f**, **56a–b**, **57**, **58a–f** and **59b,d** (Scheme 18). Despite the outstanding overall potency (XO inhibition and anti-inflammatory) of the selected compounds (Table 15), the in vitro biological assays revealed, for all the compounds, XO inhibition IC_{50} in the nanomolar range of 9–77 nM, compared to the control drug febusostat ($\text{IC}_{50} = 26$ nM). For the anti-inflammatory potential, measured by cyclooxygenase 1 and 2 (COX-1 and COX-2) inhibition, all the compounds achieved excellent IC_{50} values compared to the range expressed by the control drugs celecoxib ($\text{IC}_{50} = 14.7$ μM and 0.05 μM , for COX-1 and 2, respectively) and diclofenac sodium ($\text{IC}_{50} = 3.80$ μM and 0.84 μM , for COX-1 and 2, respectively).



Scheme 18. Different functionalized febuxostat derivatives **55a–f**, **56a–b**, **57**, **58a–f** and **59b,d** in the carboxylic acid termination [54].

Table 15. In vitro assay results for the febuxostat-based, different functionalized at carboxylic acid termination, and selected compounds activities against XO, COX-1 and COX-2 [54].

Compound	XO IC ₅₀ (nM)	COX-1 IC ₅₀ (μM)	COX-2 IC ₅₀ (μM)	COX-2 SI ^a
Celecoxib	n.t.	14.7	0.05	294
Diclofenac Na	n.t.	3.80	0.84	4.52
Febuxostat	26	5.37	0.34	15.79
55a	17	12.57	0.04	314.25
56b	11	9.63	0.07	137.57
57	9	7.37	0.14	52.64
58c	18	12.27	0.05	245.40
58e	19	12.77	0.04	319.25
59b	18	13.47	0.04	336.75

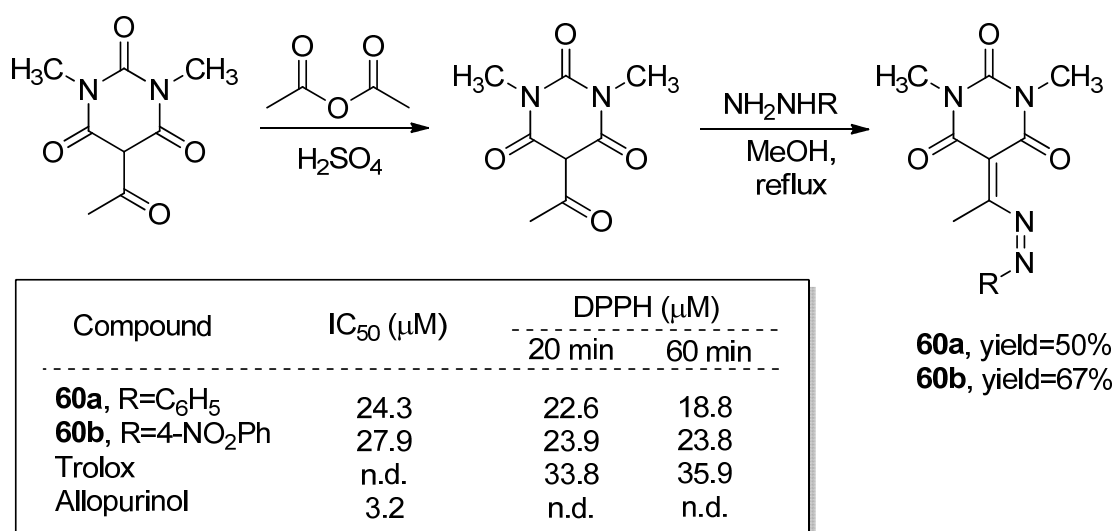
^a COX-1 IC₅₀/COX-2 IC₅₀; n.t. = not tested.

In vivo assays for hypouricemic activities of the most active in vitro compounds were carried under a potassium oxonate-induced acute hyperuricemia mouse model. The results indicated excellent serum uric acid reduction (52.53–59.60%, for a 4h treatment regimen with 5 mg/kg intragastrical administration) compared to the control drug febuxostat (48.48%). For anti-inflammatory activity, the carrageenan-induced mouse paw edema bioassay highlighted compounds **55a**, **58e** and **59b** to be equipotent or more potent than the positive control drug celecoxib in a 5 mg/kg dose over an 8h treatment regimen. Moreover, in silico studies showed that, among the selected compounds, only **56b**, **58c** and **59b** violated a Lipinski's Rule, detaining LogP >5 [54].

3.2.2. XO Inhibition and ROS Control in a Single Moiety

Given the ROS production during XO activity (Figure 1), the obtainment of XO inhibitor derivatives that are also able to exhibit ROS activity modulation can be the key chemotherapy agents for cancer and other XO-related diseases, already punctuated in the introduction, due to its bifunctionality.

Aiming at the exploration of barbiturates' wide range of biological activities expressed by enzyme inhibition, Figueiredo and coworkers [55] synthesized a vast series of 1,3,5-trisubstituted barbiturates and thiobarbiturates. Among them, two compounds, already synthesized back in 2001 by Jursic and Neumann [56], demonstrated a very interesting combination of biological activities and became of interest to this review (Scheme 19). Derivatives **60a** and **60b** presented good in vitro IC₅₀ values of 24.3 μM and 27.9 μM for XO, respectively. However, the greater antioxidant capacity than the reference drug Trolox, pointed out by the 2,2-diphenyl-1-picrylhydrazyl (DPPH) radical scavenging assay at both time intervals, put **60a** and **60b** in a special position for XO-related diseases. Given the ROS production during XO activity, both hydrazinyl derivatives can be the key compounds for cancer and other XO-related diseases, already punctuated in the introduction, treatment due to their bifunctionality.



Scheme 19. Barbiturates **60a** and **60b** in vitro potential for XO inhibition and in vitro antioxidant potential. n.d. = not determined [55].

Present in *Radix Salviae Miltiorrhizae*, salvianolic acid C (SAC) was found, by Ph.D. Chen's research group, to be a promising natural compound suitable for XO inhibition [57]. Later, in two subsequent works from the same group, Tang and coworkers vastly explored the obtained natural product through an in depth study of the SAR involved in 2-arylbenzo[b]furan molecular scaffold regarding XO inhibition [58,59]. We highlight from the 2-arylbenzo[b]furan derivatives **61a–f**, **62a–f**, **63a–f** and **64a–f** synthesized in the first work [58] (Scheme 20), the amino derivatives (**59a–f**, **60a–f**) prepared from SAC's

Table 16. 2-arylbenzo[b]furan derivatives **61a–f**, **62a–f**, **63a–f** and **64a–f** inhibitory and antioxidant activity [58].

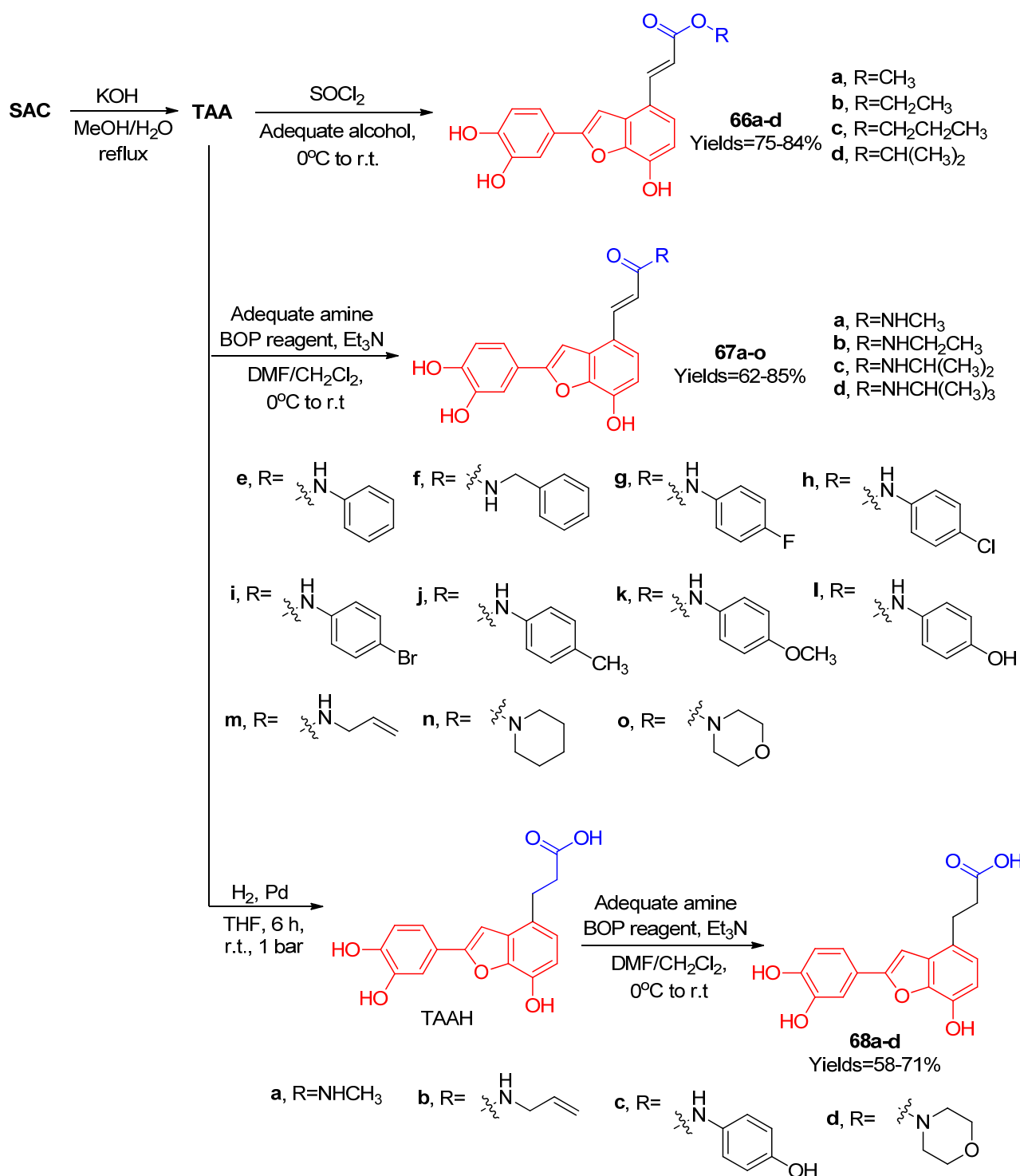
Compound	IC ₅₀ (μM)		Compound	IC ₅₀ (μM)	
	XO Inhibition	DPPH Assay		XO Inhibition	DPPH Assay
Allopurinol	3.61	n.a.	SAC	8.26	6.87
61a	9.88	8.79	62a	4.81	4.52
61b	3.99	3.9	62b	12.12	5.61
61c	10.8	11.95	62c	6.36	3.27
61d	14.91	8.66	62d	6.04	4.2
61e	13.48	47.25	62e	4.51	6.47
61f	31.72	12.37	62f	4.98	3.86
63a-f and 64a-f	>60	*	Quercetin	n.a.	6.0

* = disregarded for this work given the non-significant XO inhibition IC₅₀ values compared to control drug Allopurinol; n.a. = not applicable.

From the second work [59], novel amino derivatives were synthesized, **66a–d**, **67a–o**, and **68a–d** (Scheme 21). Among them, special attention was given to the hydrogenated TAA derivative (TAAH), with in vitro IC₅₀ = 9.76 μM lower than its preceding compound (in vitro IC₅₀ = 16.05 μM). Unfortunately, further deviations in TAAH (**68a–d**) did not result in any potency increase for XO inhibition (Table 17). Among the most potent compounds, **67a** had its efficacy in reverting the hyperuricemia condition verified in vivo with a potassium oxonate-induced hyperuricemic mice model. Kinetic assays comprising **67a** gave the same results as the first work, a mixed-type competitive mode inhibitor with respect to xanthine for binding to XO. The inhibition constant for the **67a**-enzyme complex was lower (K_i = 3.52 μM) than the one for the **67a**-enzyme-xanthine complex (K_i = 13.14 μM), showing greater inhibitor affinity for the free enzyme than for the complex. Every synthesized derivative presented good antioxidant potential in a DPPH radical scavenging assay, with IC₅₀ varying between 6.61–21.08 μM. Intracellular ROS inhibitory assays pointed out that some of the most potent inhibitors (**67a,f,n**) also presented potent ROS scavenging potential up to 10 μM.

Table 17. 2-arylbenzo[b]furan derivatives **66a–d**, **67a–d** and **68a–d** in vitro inhibitory and antioxidant activity in terms of IC₅₀ [59].

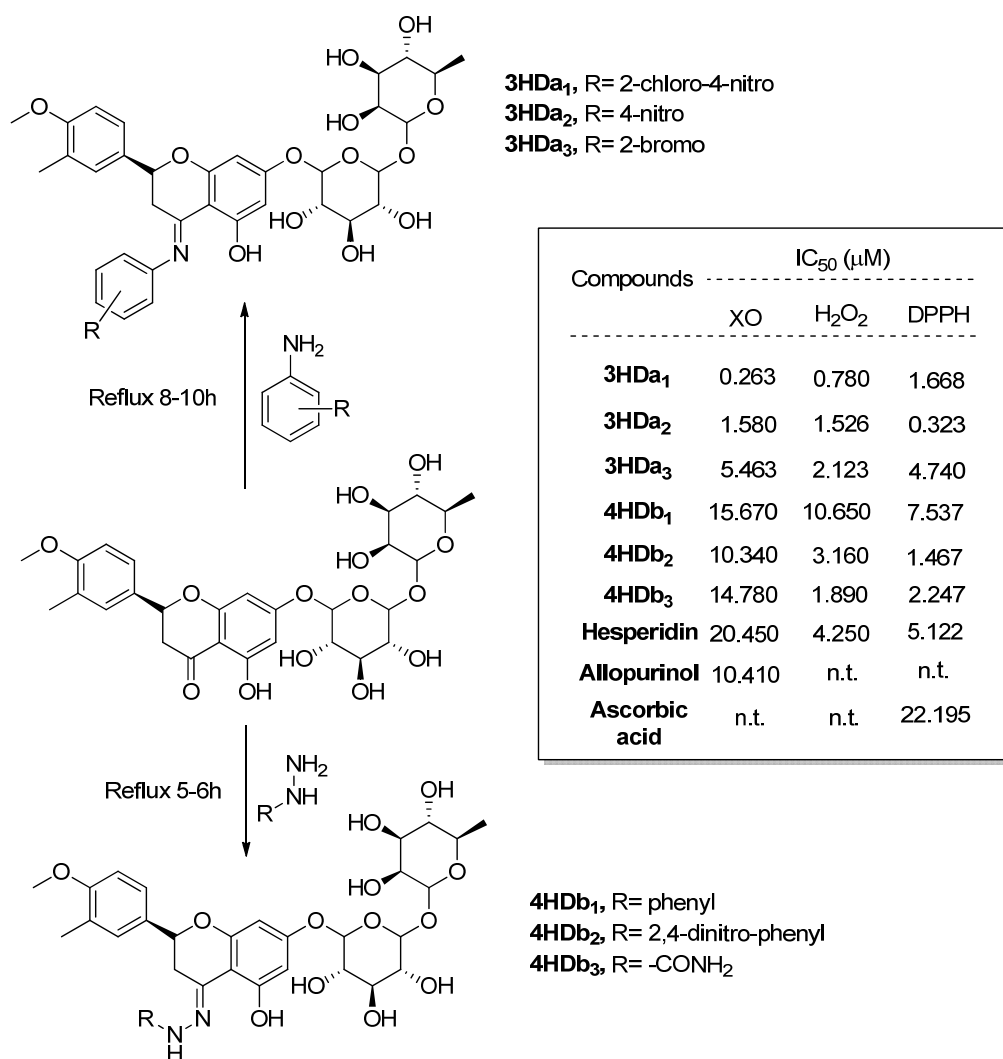
Compound	IC ₅₀ (μM)	Compound	IC ₅₀ (μM)
	XO Inhibition		XO Inhibition
Allopurinol	10.61	TAA	16.05
66a	6.55	66b	15.46
66c	19.31	66d	24.17
67a	4.45	67b	13.49
67c	13.86	67d	45.18
67e	17.84	67f	15.55
67g	83.81	67h	>100
67i	>100	67j	51.28
67k	42.19	67l	11.01
67m	18.16	67n	11.01
67o	>100	TAAH	9.76
68a	11.47	68b	46.79
68c	38.59	68d	>100



Scheme 21. Synthesis protocol for the obtainment of the 2-arylbenzo[b]furan derivatives **66a–d**, **67a–d** and **68a–d** [59].

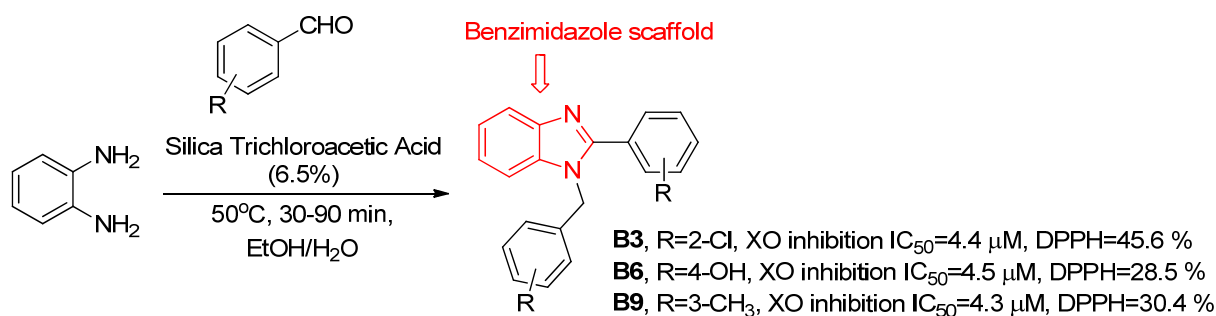
In a previous work, Malik and coworkers [60] have found, through in silico design and ADMET studies, that hesperidin succeeded as a potential XO inhibitor. Already being known for its antioxidant potential, in a second work [61] novel hydrazine and amine hesperidin derivatives were synthesized as XO inhibitors and antioxidant agents (Scheme 22). The synthesized compounds have shown good XO inhibition activity, the most promising one being 3HD_{a1}. It showed an in vitro XO inhibition activity up to 50 times better than the positive control drug, allopurinol (IC₅₀ = 10.410 μM), nearly 100 times

better than the precursor compound hesperidin ($IC_{50} = 20.450 \mu M$), and was also one of the most potent in the antioxidant assays. A molecular docking study was carried out with the two most potent compounds (3HDA₁ and 3HDA₂). It pointed out that their main interactions with XO were the same, with the exception of the O-glycoside OH group with Gly1260 (3HDA₁) and phenolic ring OH group with Thr592 (3HDA₂). Only one polar interaction with Gln585 was found to be the same for 3HDA₁, 3HDA₂, and hesperidin. Regarding SAR studies, it is pointed out that, overall, amino derivatives proved to be more promising than the hydrazine ones. Moreover, the electron-withdrawing group at the aromatic ring seems to enhance the bioactivities. Lastly, the kinetic assays assigned 3HDA₁ as a competitive inhibitor.



Scheme 22. Hesperidin derivatives (3HDA₁₋₃ and 4HDb₁₋₃) synthesis and its in vitro XO inhibition, H₂O₂ and DPPH radical scavenging potential in terms of IC₅₀ [61].

Benzimidazole moiety is known for its broad biological activities, ranging from anticancer, to antioxidant [62,63]. Therefore, Nile and coworkers [64] have synthesized a collection of benzimidazole derivatives as novel XO inhibitors, that also act as a free radical scavenger. We highlight the three most active ones (B3, B6, B9) (Scheme 23), which presented an in vitro IC₅₀ lower than the standard allopurinol (IC₅₀ = 5.5 μM). Moreover, a potential antioxidant activity, reaching almost the same radical scavenging activity in the DPPH assay as the control compound quercetin (48,8%), was observed.



Scheme 23. Synthesized benzimidazoles derivatives (B3, B6, B9) and their in vitro XO activity in terms of IC_{50} and antioxidant activity [64].

4. IMER Based HPLC and CE Assays to Screen for XO Inhibitors

The advent of enzyme immobilization in solid supports started a new trend in bioactive compounds screening. By using adequately treated capillaries, enzymes became available as a viable stationary phase once immobilized into their surface. The obtained piece is called an immobilized enzyme reactor (IMER) where the stationary phase can selectively interact with substrates and inhibitors [20]. This selectivity is particularly attractive when considering the complexity regarding the presence of dozens of compounds in natural or synthetic complex matrices for unveiling novel potential pharmacological entities. Separating and purifying each one of them is completely out of scope, especially when their exact number is unknown, and the additional step of individual structure characterization would require an extraordinary effort and amount of time [65]. Moreover, a remarkable characteristic of IMERs is the possibility of multiple uses of the same enzymes, considerably reducing the biological assays costs [66].

Therefore, in-flow screening assay systems provide a plethora of benefits to elegantly overcome this challenge. Overall, we can highlight being a single and automatized procedure that can separate the components, identify the bioactive ones and quantify its efficiency. Consequently, this kind of assay allows the obtainment of an inhibition constant (K_i), inhibition mechanism, and Michaelis–Menten constant (K_M) [22]. Specific discussion regarding the obtainment of those analytical data and the chemistry involved in the IMER manufacturing will not be described, once there are already a plethora of articles doing so [20,22,24,66–69], and it will drift away from this article's purpose regarding XO.

4.1. HPLC Approaches

Rodrigues and coworkers [70] adapted an HPLC system where an IMER consisting of a fused silica capillary, amino-functionalized with (3-aminopropyl)triethoxysilane (APTES) and treated with glutaraldehyde (GA) to covalently bind the enzymes was employed in a unidimensional assay. Despite an IMER detaining no resolution, the coupled tandem MS as the detection method allowed the unambiguous identification of XO inhibitors at a rate of 288 analysis/day (Figure 2A). This way, thirty natural compounds from different sources were screened, and their respective inhibition percentages and IC_{50} values were obtained based on the IMER activity modulation as a consequence of the injected compound. Moreover, with the injection of crescent concentrations of substrate (xanthine), $K_M = 14.5 \mu$ M was accessed by nonlinear regression of the Michaelis–Menten plots. A previous setup [71] consisted of a bidimensional HPLC system with an analytical C18 column in the second dimension, so the DAD detector was able to be used. Despite being a cheaper and easier-to-work setup, this 2D-HPLC approach slowed down the screening to a rate of 84 analyses/day (Figure 2B). A series of ruthenium complexes based on the allopurinol structure was able to be successfully screened. The derivative 4CBALO presented $K_i = 0.29 \mu$ M and $IC_{50} = 0.07 \mu$ M, more than five times and 4.5 times lower than allopurinol ($K_i = 1.55 \mu$ M and $IC_{50} = 0.32 \mu$ M), respectively. Moreover, with the IMER activity being

able to be recovered up to 97%, together with the low K_i and IC_{50} values, 4CBALO was characterized as a reversible competitive tight-binding XO inhibitor.

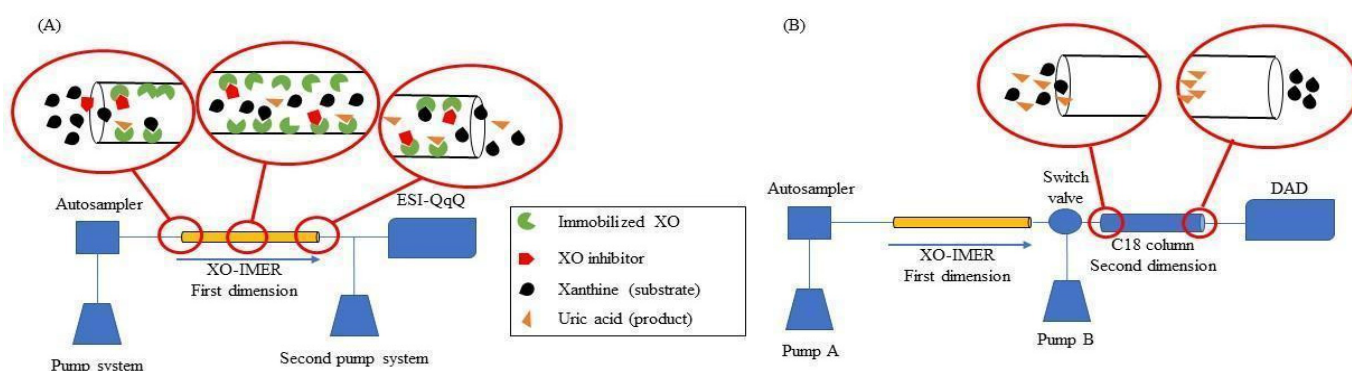
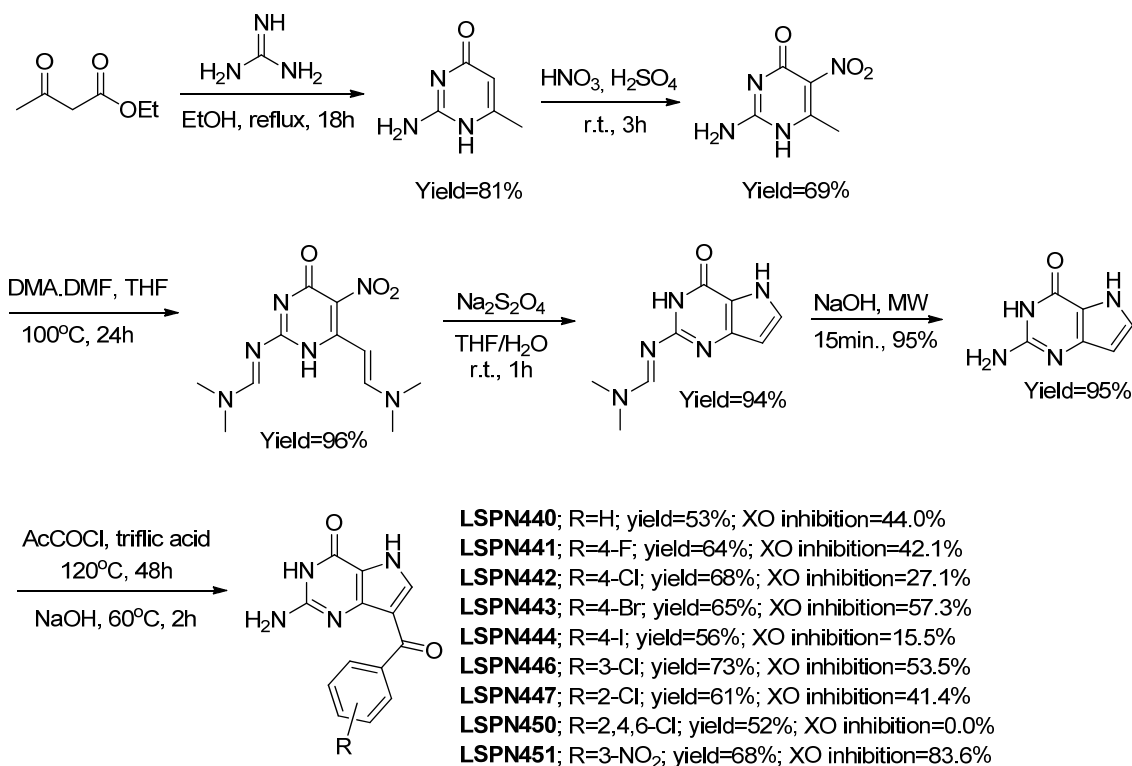


Figure 2. (A) Unidimensional and (B) bidimensional HPLC approaches for in-flow screening of XO inhibitors.

Using the same setup for the screening of the ruthenium complexes, nine synthesized deazaguanine derivatives (Scheme 24), based on allopurinol's molecular skeleton, were able to be screened for their XO inhibition potential [72]. Among them, LSPN451 was observed to be a promising candidate for additional assays given its more pronounced enzymatic activity modulation by inhibiting 83.6% of the IMER's activity, thus reducing the produced UA. LSPN4451 $IC_{50} = 65$ nM was retrieved from an inhibition curve constructed by varying the given inhibitor concentration at a fixed substrate concentration. The non-competitive inhibition mechanism and inhibition constant $K_i = 55.1$ nM (almost thirty times more potent than allopurinol for the same assay) were extracted from the Lineweaver–Burk plot constructed with different concentrations of the substrate for each injection of pre-determined inhibitor concentrations.



Scheme 24. Synthesized deazaguanines derivatives screened for XO inhibition and its inhibition efficiency [72].

Using the same 2D-HPLC setup previously described, Peng and coworkers [73] managed to adequately produce an automatized platform to execute solid-phase ligand-fishing in the first dimension IMER, followed by separation, purification, and quantification in the second dimension C-18 analytic column. After injection, the sample was eluted by the buffer employed as the initial mobile phase, so that unbound compounds were flushed out while XO inhibitors stayed inside the IMER. In a second moment, the programmed valve switched. Therefore, methanol became the mobile phase and the bounded compounds were carried to the analytical column. It should be mentioned that even after the methanol wash, the IMER retained 96% of its activity after ten consecutive cycles. Under those conditions, six compounds could be fished out from the *Lonicera macranthoides* extract and identified, after retention time, UV and MS/MS analysis, namely caffeoylquinic acid, 5-caffeoylquinic acid, 4-caffeoylquinic acid, 3,4-dicaffeoylquinic acid, 3,5-dicaffeoylquinic acid, and 4,5-dicaffeoylquinic acid.

4.2. CE Approaches

CE is a separation technique where the components present in a sample matrix migrate at different speeds, either qualitatively or quantitatively, through the application of a potential difference between two immersed electrodes in an ionic solution. Due to its low sample consumption, ability to monitor the reaction in real-time, the potential for high throughput and high resolving power, CE is also used for screening enzyme inhibitors through voltage difference separation followed by direct detection and quantification of the enzymatic product considering an in-flow approach [74,75].

CE was successfully used by Wu and coworkers [23] for in-flow screening natural compounds as XO inhibitors. After XO immobilization in the fused silica capillary (Figure 3), different substrate concentrations were injected to perform kinetic studies that allowed the obtainment of $K_M = 0.39$ mM, being considered by the authors as a close value to the one described in the literature value, showing no significant structural changes in XO after immobilization. The K_i of 5.2 μM was also obtained using the known XO inhibitor 4-aminopyrazolo[3,4-d]pyrimidine (4APP), slightly lower than the literature (8 μM), which was acceptable and justified by enzymes origin and assay conditions. Lastly, in under 5 min screening assays, four of the ten flavonoids showed promising results ($>50\%$ inhibition of XO activity) through the in-flow methodology, namely dihydroquercetin, quercetin, biochanin A, and epicatechin. The IMER maintained up to 95% of its enzymatic activity after thirty consecutive assays.

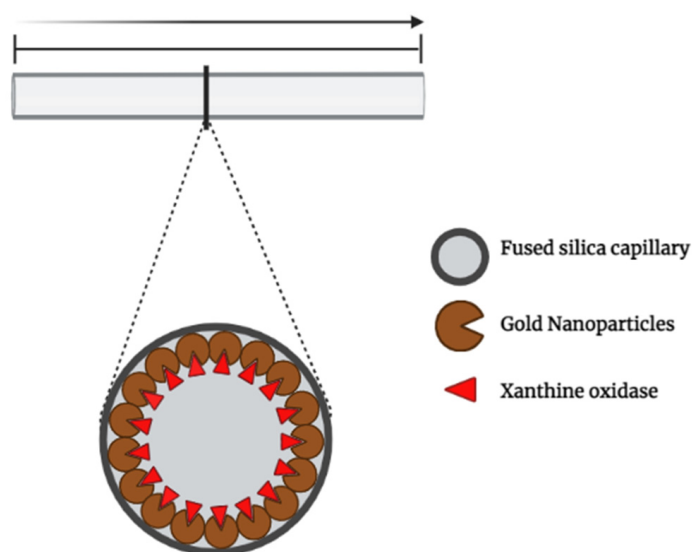


Figure 3. Capillary for CE containing gold nanoparticles with immobilized XO for inhibitors screening [23].

Pingtan and coworkers [75] also developed an in-flow method for XO inhibitors screening using CE, but with adenosine deaminase (ADA) co-immobilization in the same IMER to identify possible inhibitors from a library of 20 natural extracts (Figure 4). Co-immobilization was performed with both negatively charged enzymes on gold nanoparticles, and later, they were immobilized at the entrance end of the positively charged capillary by electrostatic interactions. After immobilization in the capillary, different substrates concentration injections allowed the obtainment of the calculated K_M of 0.55 mM for ADA and 0.37 mM for XO. Those values were reported by the authors to be different from the literature, but acceptable and justifiable by means of changes in affinity between the enzyme-substrate due to the immobilization process. Kinetic tests were performed with known inhibitors, erythro-9-(2-hydroxy-3-nonyl)adenine for ADA and 4APP for XO. The method was validated by the calculated K_i values of 9.6 nM and 8.9 μ M, which matched the literature-reported ones. Screening assays that took less than 3 min pointed to the extract of rhizoma chuanxiong and indigo naturalis as ADA inhibitors, while the extract of rhizoma chuanxiong, cortex phellodendri, rhizoma alpiniae officinarum, and ramulus cinnamoni were identified as XO inhibitors, concluding that the extract of rhizoma chuanxiong is an inhibitor of both enzymes. Therefore, the developed method also proved to be a promising multi-target enzyme screening method.

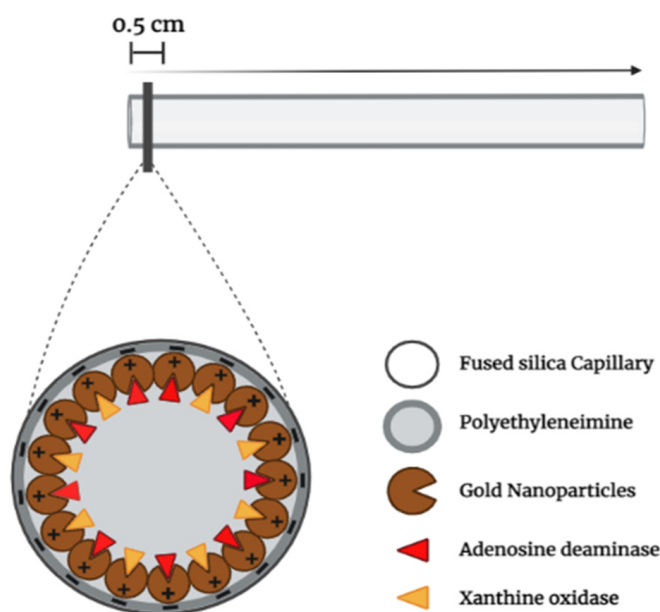


Figure 4. XO and ADA co-immobilized in gold nanoparticles inside the initial portion of a capillary for inhibitors screening by CE [75].

5. Conclusions

Many advances comprising the obtainment of XO inhibitors were observed. Novel synthetic febuxostat-based inhibitors were reported with IC_{50} and inhibition rate as good as the FDA-approved drugs employed as control (Allopurinol and Febuxostat). Hybridization and isosterism were used as the main synthetic gimmicks to obtain the more potent derivatives. Under this concept, heterocyclic rings allowed the synthesis of a plethora of high potency inhibitors, which ranked them into a privileged position as a viable molecular scaffold to develop further XO inhibitors. Additionally, molecular modeling studies allowed further comprehension of the key molecular features, which an effective molecular framework should present to behave as a potential XO inhibitor, allowing, in some cases, the achievement of nanomolar potencies and kinetic assays that pointed out that the most potent derivatives presented mixed-type inhibition mechanism. Together, synthetic and computational works are closing the gap for the obtainment of more potent

and selective small molecules that behave as XO inhibitors. In short, aiming for structural changes over hybridization leads to more derivatives bearing a nanomolar range of potency. However, a more complex challenge seems to have been established over the last decade, as bifunctional compounds have been produced to inhibit XO activity and at the same time control aggravating factors associated with its activity like ROS and inflammatory process control.

On the other hand, developments in biological assays allowed the obtainment of screening techniques comprising the combination of enzymes, a very delicate and expensive resource, with high-end analytical instruments with automated operation (HPLC and CE). That association enabled the achievement of powerful and versatile setups to screen for XO inhibitors in natural sources without the necessity of individual steps of separation, purification or identification, accelerating the discovery of unknown XO inhibitor compounds. Additionally, the adequate approach made the acquisition of kinetic parameters (K_M and K_i), the mechanism (competitive, uncompetitive and non-competitive), and potency (IC_{50} and inhibition rates) in single automatized procedures possible. Lastly, IMERs allowed the manutention of enzymes' stability and activity for several assays, reducing the drug discovery process costs, differently to the one-time use only for solution assays.

Author Contributions: Conceptualization, R.C.S.L.; methodology, R.C.S.L. and C.A.W.; validation, R.C.S.L.; formal analysis, R.C.S.L. and C.A.W.; investigation, R.C.S.L. and C.A.W.; data curation, M.F.S.d.A., C.A.W., M.S.C., I.G.M.S. and R.C.S.L.; writing—original draft preparation, M.F.S.d.A., C.A.W., M.S.C., I.G.M.S. and R.C.S.L.; writing—review and editing, R.C.S.L.; supervision, R.C.S.L. All authors have read and agreed to the published version of the manuscript.

Funding: This study was financed in part by the Coordenação de Aperfeiçoamento de Pessoal de Nível Superior—Brasil (CAPES)—Finance Code 001. CNPq and FAPERJ (Grants E-26/202.909/2019, E-26/010.000978/2019 and SEI-260003/001167/2020).

Data Availability Statement: Not applicable.

Acknowledgments: Renato C. S. Lessa acknowledges Coordenação de Aperfeiçoamento de Pessoal de Nível Superior—Brasil (CAPES) for the scholarship received. Miguel F. S. de Abreu and Camila A. Wegermann acknowledges Fundação Carlos Chagas Filho de Amparo à Pesquisa do Estado do Rio de Janeiro (FAPERJ) for the scholarship received.

Conflicts of Interest: The authors declare no conflict of interest.

References

1. McManaman, J.L.; Bain, D.L. Structural and Conformational Analysis of the Oxidase to Dehydrogenase Conversion of Xanthine Oxidoreductase. *J. Biol. Chem.* **2002**, *277*, 21261–21268. [[CrossRef](#)] [[PubMed](#)]
2. Hille, R.; Hall, J.; Basu, P. The Mononuclear Molybdenum Enzymes. *Chem. Rev.* **2014**, *114*, 3963–4038. [[CrossRef](#)] [[PubMed](#)]
3. Pacher, P.; Nivorozhkin, A.; Szabó, C. Therapeutic Effects of Xanthine Oxidase Inhibitors: Renaissance Half a Century after the Discovery of Allopurinol. *Pharmacol. Rev.* **2006**, *58*, 87–114. [[CrossRef](#)]
4. Ty, M.C.; Zuniga, M.; Gotz, A.; Sahu, P.K.; Mohanty, A.; Mohanty, S.; Wassmer, S.C.; Rodriguez, A. Malaria inflammation by xanthine oxidase-produced reactive oxygen species. *EMBO Mol. Med.* **2019**, *11*, e9903. [[CrossRef](#)] [[PubMed](#)]
5. Iwalokun, B.A.; Bamiro, S.B.; Ogunledun, A. Levels and interactions of plasma xanthine oxidase, catalase and liver function parameters in Nigerian children with Plasmodium falciparum infection. *APMIS* **2006**, *114*, 842–850. [[CrossRef](#)] [[PubMed](#)]
6. Luchtemberg, M.N.; Petronilho, F.; Constantino, L.; Gelain, D.P.; Andrades, M.; Ritter, C.; Moreira, J.C.F.; Streck, E.L.; Dal-Pizzol, F. Xanthine oxidase activity in patients with sepsis. *Clin. Biochem.* **2008**, *41*, 1186–1190. [[CrossRef](#)] [[PubMed](#)]
7. Schmidt, H.M.; Kelley, E.E.; Straub, A.C. The impact of xanthine oxidase (XO) on hemolytic diseases. *Redox Biol.* **2019**, *21*, 101072. [[CrossRef](#)]
8. Hassoun, P.M.; Yu, F.S.; Gote, C.G.; Zulueta, J.J.; Sawhney, R.; Skinner, K.A.; Skinner, H.B.; Parks, D.A.; Lanzillo, J.J. Upregulation of Xanthine Oxidase by Lipopolysaccharide, Interleukin-1, and Hypoxia. *Am. J. Respir. Crit. Care Med.* **1998**, *158*, 299–305. [[CrossRef](#)]
9. Komakia, Y.; Sugiuraa, H.; Koarai, A.; Tomaki, M.; Ogawa, H.; Akita, T.; Hattori, T.; Ichinose, M. Cytokine-mediated xanthine oxidase upregulation in chronic obstructive pulmonary disease's airways. *Pulm. Pharmacol. Ther.* **2005**, *18*, 297–302. [[CrossRef](#)]
10. Akhigbe, R.E.; Ajayi, L.O.; Ajayi, A.F. Codeine exerts cardiorenal injury via upregulation of adenine deaminase/xanthine oxidase and caspase 3 signaling. *Life Sci.* **2021**, *273*, 118717. [[CrossRef](#)] [[PubMed](#)]

11. Jinnah, H.A.; Sabina, R.L.; Berghe, G.V.D. Metabolic disorders of purine metabolism affecting the nervous system. *Handb. Clin. Neurol.* **2013**, *113*, 1827–1836.
12. Bove, M.; Cicero, A.F.; Borghi, C. The Effect of Xanthine Oxidase Inhibitors on Blood Pressure and Renal Function. *Curr. Hypertens. Rep.* **2017**, *19*, 95. [[CrossRef](#)] [[PubMed](#)]
13. Kim, S.C.; Schneeweiss, S.; Choudhry, N.; Liu, J.; Glynn, R.J.; Solomon, D.H. Effects of Xanthine Oxidase Inhibitors on Cardiovascular Disease in Patients with Gout: A Cohort Study. *Am. J. Med.* **2015**, *128*, 653.e7–653.e16. [[CrossRef](#)]
14. Dawson, J.; Walters, M. Uric acid and xanthine oxidase: Future therapeutic targets in the prevention of cardiovascular disease? *Br. J. Clin. Pharmacol.* **2006**, *62*, 633–644. [[CrossRef](#)] [[PubMed](#)]
15. Saito, H.; Tanaka, K.; Iwasaki, T.; Oda, A.; Watanabe, S.; Kanno, M.; Kinura, H.; Shimabukuro, M.; Asahi, K.; Watanabe, T.; et al. Xanthine oxidase inhibitors are associated with reduced risk of cardiovascular disease. *Sci. Rep.* **2021**, *11*, 1380. [[CrossRef](#)]
16. Borges, F.; Fernandes, E.; Roleira, F. Progress Towards the Discovery of Xanthine Oxidase Inhibitors. *Curr. Med. Chem.* **2002**, *9*, 195–217. [[CrossRef](#)] [[PubMed](#)]
17. Wright, D.T.; Cohn, L.A.; Li, H.; Fischer, B.; Li, M.L.; Adler, K.B. Interactions of Oxygen Radicals with Airway Epithelium. *Environ. Health Perspect.* **1994**, *102*, 85–90. [[PubMed](#)]
18. Zádák, Z.; Hyspler, R.; Tichá, A.; Hronek, M.; Fikrová, P.; Rathouská, J.; Hrnčiariková, D.; Stetina, R. Antioxidants and vitamins in clinical conditions. *Physiol. Res.* **2009**, *58*, S13–S17. [[CrossRef](#)] [[PubMed](#)]
19. Copeland, R.A.; Harpel, M.R.; Tummino, P.J. Targeting enzyme inhibitors in drug discovery. *Expert Opin. Ther. Targets* **2007**, *11*, 967–978. [[CrossRef](#)] [[PubMed](#)]
20. De Moraes, M.C.; Cardoso, C.L.; Cass, Q.B. Solid-Supported Proteins in the Liquid Chromatography Domain to Probe Ligand-Target Interactions. *Front. Chem.* **2019**, *7*, 752. [[CrossRef](#)] [[PubMed](#)]
21. Ximenes, I.A.; Albino, M.; Sangregorio, C.; Cass, Q.B.; de Moraes, M.C. On-flow magnetic particle activity assay for the screening of human purine nucleoside phosphorylase inhibitors. *J. Chromatogr. A* **2022**, *1663*, 462740. [[CrossRef](#)]
22. Calleri, E.; Temporini, C.; Colombo, R.; Tengattini, S.; Rinaldi, F.; Brusotti, G.; Furlanetto, S.; Massolini, G. Analytical settings for in-flow biocatalytic reaction monitoring. *Trends Anal. Chem.* **2021**, *143*, 116348. [[CrossRef](#)]
23. Wu, Z.Y.; Zhang, H.; Yang, Y.Y.; Yang, F.Q. Evaluation of xanthine oxidase inhibitory activity of flavonoids by an on-line capillary electrophoresis-based immobilized enzyme microreactor. *Electrophoresis* **2020**, *41*, 1326–1332. [[CrossRef](#)]
24. De Simone, A.; Naldi, M.; Bartolini, M.; Davani, L.; Andrisano, V. Immobilized Enzyme Reactors: An Overview of Applications in Drug Discovery from 2008 to 2018. *Chromatographia* **2019**, *82*, 425–441. [[CrossRef](#)]
25. Kelley, E.E.; Trostchansky, A.; Rubbo, H.; Freeman, B.A.; Radi, R.; Tarpey, M.M. Binding of Xanthine Oxidase to Glycosaminoglycans Limits Inhibition by Oxypurinol. *J. Biol. Chem.* **2004**, *279*, 37231–37234. [[CrossRef](#)] [[PubMed](#)]
26. Shi, A.; Zhang, L.; Wang, H.; Wang, S.; Yang, M.; Guan, Q.; Bao, K.; Zhang, W. Design, synthesis and bioevaluation of 2-mercapto-6-phenylpyrimidine-4-carboxylic acid derivatives as potent xanthine oxidase inhibitors. *Eur. J. Med. Chem.* **2018**, *155*, 590–595. [[CrossRef](#)] [[PubMed](#)]
27. Komoriya, K.; Osada, Y.; Hasegawa, M.; Horiuchi, H.; Kondo, S.; Couch, R.C.; Griffin, T.B. Hypouricemic effect of allopurinol and the novel xanthine oxidase inhibitor TEI-6720 in chimpanzees. *Eur. J. Pharmacol.* **1993**, *250*, 455–460. [[CrossRef](#)]
28. Osada, Y.; Tsuchimoto, M.; Fukushima, H.; Kondo, S.; Hasegawa, M.; Komoriya, K. Hypouricemic effect of the novel xanthine oxidase inhibitor, TEI-6720, in rodents. *Eur. J. Pharmacol.* **1993**, *241*, 183–188. [[CrossRef](#)]
29. Robinson, C.P.; Dalbeth, N. Febuxostat for the treatment of hyperuricaemia in gout. *Expert Opin. Pharmacother.* **2018**, *19*, 1289–1299. [[CrossRef](#)]
30. Grewal, H.K.; Martinez, J.R.; Espinoza, L.R. Febuxostat: Drug review and update. *Expert Opin. Drug Metab. Toxicol.* **2014**, *10*, 747–758. [[CrossRef](#)] [[PubMed](#)]
31. Okamoto, K.; Eger, B.T.; Nishino, T.; Kondo, S.; Pai, E.F.; Nishino, T. An extremely potent inhibitor of xanthine oxidoreductase. Crystal structure of the enzyme-inhibitor complex and mechanism of inhibition. *J. Biol. Chem.* **2003**, *278*, 1848–1855. [[CrossRef](#)] [[PubMed](#)]
32. Fukunari, A.; Okamoto, K.; Nishino, T.; Eger, B.T.; Pai, E.F.; Kamezawa, M.; Yamada, I.; Kato, N. Y-700 [1-[3-Cyano-4-(2,2-dimethylpropoxy)phenyl]-1H-pyrazole-4-carboxylic acid]: A potent xanthine oxidoreductase inhibitor with hepatic excretion. *J. Pharmacol. Exp. Ther.* **2004**, *311*, 519–528. [[CrossRef](#)] [[PubMed](#)]
33. Ishibuchi, S.; Morimoto, H.; Oe, T.; Ikebe, T.; Inoue, H.; Fukunari, A.; Kamezawa, M.; Yamada, I.; Naka, Y. Synthesis and structure-activity relationships of 1-phenylpyrazoles as xanthine oxidase inhibitors. *Bioorg. Med. Chem. Lett.* **2001**, *11*, 879–882. [[CrossRef](#)]
34. Ding, H.X.; Leverett, C.A.; Kyne, R.E., Jr.; Liu, K.K.-C.; Fink, S.J.; Flick, A.C.; O'Donnell, C.J. Synthetic approaches to the 2013 new drugs. *Bioorg. Med. Chem.* **2015**, *23*, 1895–1922. [[CrossRef](#)]
35. Sato, T.; Ashizawa, N.; Matsumoto, K.; Iwanaga, T.; Nakamura, H.; Inoue, T.; Nagata, O. Discovery of 3-(2-cyano-4-pyridyl)-5-(4-pyridyl)-1,2,4-triazole, FYX-051-a xanthine oxidoreductase inhibitor for the treatment of hyperuricemia. *Bioorg. Med. Chem. Lett.* **2009**, *19*, 6225–6229. [[CrossRef](#)]
36. Matsumoto, K.; Okamoto, K.; Ashizawa, N.; Nishino, T. FYX-051: A novel and potent hybrid-type inhibitor of xanthine oxidoreductase. *J. Pharmacol. Exp. Ther.* **2011**, *336*, 95–103. [[CrossRef](#)]
37. Nishino, T.; Okamoto, K. Mechanistic insights into xanthine oxidoreductase from development studies of candidate drugs to treat hyperuricemia and gout. *J. Biol. Inorg. Chem.* **2015**, *20*, 195–207. [[CrossRef](#)]

38. Song, J.U.; Choi, S.P.; Kim, T.H.; Jung, C.K.; Lee, J.-Y.; Jung, S.-H.; Kim, G.T. Design and synthesis of novel 2-(indol-5-yl)thiazole derivatives as xanthine oxidase inhibitors. *Bioorg. Med. Chem. Lett.* **2015**, *25*, 1254–1258. [[CrossRef](#)]
39. Guan, Q.; Cheng, Z.; Ma, X.; Wang, L.; Feng, D.; Cui, Y.; Bao, K.; Wu, L.; Zhang, W. Synthesis and bioevaluation of 2-phenyl-4-methyl-1,3-selenazole-5-carboxylic acids as potent xanthine oxidase inhibitors. *Eur. J. Med. Chem.* **2014**, *85*, 508–516. [[CrossRef](#)]
40. Li, J.; Wu, F.; Liu, X.; Zou, Y.; Chen, H.; Li, Z.; Zhang, L. Synthesis and bioevaluation of 1-phenyl-pyrazole-4-carboxylic acid derivatives as potent xanthine oxidoreductase inhibitors. *Eur. J. Med. Chem.* **2017**, *140*, 20–30. [[CrossRef](#)]
41. Chen, S.; Zhang, T.; Wang, J.; Wang, F.; Niu, H.; Wu, C.; Wang, S. Synthesis and evaluation of 1-hydroxy/methoxy-4-methyl-2-phenyl-1H-imidazole-5-carboxylic acid derivatives as non-purine xanthine oxidase inhibitors. *Eur. J. Med. Chem.* **2015**, *103*, 343–353. [[CrossRef](#)] [[PubMed](#)]
42. Shi, A.; Wang, D.; Wang, H.; Wu, Y.; Tian, H.; Guan, Q.; Kai, B.; Zhang, W. Synthesis and bioevaluation of 2-phenyl-5-methyl-2H-1,2,3-triazole-4-carboxylic acid/carbohydrazide derivatives as potent xanthine oxidase inhibitors. *RSC Adv.* **2016**, *6*, 114879–114888. [[CrossRef](#)]
43. Zhang, T.J.; Wu, Q.X.; Li, S.-Y.; Wang, L.; Sun, Q.; Zhang, Y.; Meng, F.-h.; Gao, H. Synthesis and evaluation of 1-phenyl-1H-1,2,3-triazole-4-carboxylic acid derivatives as xanthine oxidase inhibitors. *Bioorg. Med. Chem. Lett.* **2017**, *27*, 3812–3816. [[CrossRef](#)] [[PubMed](#)]
44. Jyothi, M.; Khamees, H.A.; Patil, S.M.; Ramu, R.; Khanum, S.A. Microwave-Assisted Synthesis, Characterization, Docking Studies and Molecular Dynamic of Some Novel Phenyl Thiazole Analogs as Xanthine Oxidase Inhibitor. *J. Iran. Chem. Soc.* **2022**, *19*, 3919–3933. [[CrossRef](#)]
45. Zhang, T.J.; Zhang, Y.; Zhang, Z.H.; Wang, Z.R.; Zhang, X.; Hu, S.S.; Lu, P.F.; Guo, S.; Meng, F.H. Discovery of 4-(phenoxy-methyl)-1H-1,2,3-triazole derivatives as novel xanthine oxidase inhibitors. *Bioorg. Med. Chem. Lett.* **2022**, *60*, 128582. [[CrossRef](#)]
46. Zhang, L.; Wang, S.; Yang, M.; Shi, A.; Wang, H.; Guan, Q.; Bao, K.; Zhang, W. Design, synthesis and bioevaluation of 3-oxo-6-aryl-2,3-dihydropyridazine-4-carbohydrazide derivatives as novel xanthine oxidase inhibitors. *Bioorg. Med. Chem.* **2019**, *27*, 1818–1823. [[CrossRef](#)]
47. Khanna, S.; Burudkar, S.; Bajaj, K.; Shah, P.; Keche, A.; Ghosh, U.; Desai, A.; Srivastava, A.; Kulkarni-Almeida, A.; Deshmukh, N.J.; et al. Isocytosine-based inhibitors of xanthine oxidase: Design, synthesis, SAR, PK and in vivo efficacy in rat model of hyperuricemia. *Bioorg. Med. Chem. Lett.* **2012**, *22*, 7543–7546. [[CrossRef](#)]
48. Bajaj, K.; Burudkar, S.; Shah, P.; Keche, A.; Ghosh, U.; Tannu, P.; Khanna, S.; Srivastava, A.; Deshmukh, N.J.; Dixit, A.; et al. Lead optimization of isocytosine-derived xanthine oxidase inhibitors. *Bioorg. Med. Chem. Lett.* **2013**, *23*, 834–838. [[CrossRef](#)]
49. Zhang, B.; Dai, X.; Bao, Z.; Mao, Q.; Duan, Y.; Yang, Y.; Wang, S. Targeting the subpocket in xanthine oxidase: Design, synthesis, and biological evaluation of 2-[4-alkoxy-3-(1H-tetrazol-1-yl) phenyl]-6-oxo-1,6-dihydropyrimidine-5-carboxylic acid derivatives. *Eur. J. Med. Chem.* **2019**, *181*, 111559. [[CrossRef](#)]
50. Zhang, T.J.; Zhang, Y.; Tu, S.; Wu, Y.-H.; Zhang, Z.-H.; Meng, F.-H. Design, synthesis and biological evaluation of N-(3-(1H-tetrazol-1-yl)phenyl)isonicotinamide derivatives as novel xanthine oxidase inhibitors. *Eur. J. Med. Chem.* **2019**, *183*, 111717. [[CrossRef](#)]
51. Zhang, T.J.; Li, S.-Y.; Wang, L.; Sun, Q.; Wu, Q.-X.; Zhang, Y.; Meng, F.-H. Design, synthesis and biological evaluation of N-(4-alkoxy-3-cyanophenyl)isonicotinamide/nicotinamide derivatives as novel xanthine oxidase inhibitors. *Eur. J. Med. Chem.* **2017**, *141*, 362–372. [[CrossRef](#)] [[PubMed](#)]
52. Zhang, T.; Lv, Y.; Lei, Y.; Liu, D.; Feng, Y.; Zhao, J.; Chen, S.; Meng, F.; Wang, S. Design, synthesis and biological evaluation of 1-hydroxy-2-phenyl-4-pyridyl-1H-imidazole derivatives as xanthine oxidase inhibitors. *Eur. J. Med. Chem.* **2018**, *146*, 668–677. [[CrossRef](#)] [[PubMed](#)]
53. Zhang, T.J.; Li, S.Y.; Zhang, Y.; Wu, Q.X.; Meng, F.H. Design, synthesis, and biological evaluation of 5-(4-(pyridin-4-yl)-1H-1,2,3-triazol-1-yl)benzotrile derivatives as xanthine oxidase inhibitors. *Chem. Biol. Drug Des.* **2017**, *91*, 526–533. [[CrossRef](#)] [[PubMed](#)]
54. Rashad, A.Y.; Kassab, S.E.; Daabees, H.G.; Moneim, A.E.A.; Rostom, S.A.F. Febuxostat-based amides and some derived heterocycles targeting xanthine oxidase and COX inhibition. Synthesis, in vitro and in vivo biological evaluation, molecular modeling and in silico ADMET studies. *Bioorg. Chem.* **2021**, *113*, 104948. [[CrossRef](#)] [[PubMed](#)]
55. Figueiredo, J.; Serrano, J.L.; Cavalheiro, E.; Keurulainen, L.; Yli-Kauhaluoma, J.; Moreira, V.M.; Ferreira, S.; Domingues, F.C.; Silvestre, S.; Almeida, P. Trisubstituted barbiturates and thiobarbiturates: Synthesis and biological evaluation as xanthine oxidase inhibitors, antioxidants, antibacterial and anti-proliferative agents. *Eur. J. Med. Chem.* **2018**, *143*, 829–842. [[CrossRef](#)]
56. Jursic, B.S.; Neumann, D.M. Preparation of 5-formyl- and 5-acetylbarbituric acids, including the corresponding Schiff bases and phenylhydrazones. *Tetrahedron Lett.* **2001**, *42*, 8435–8439. [[CrossRef](#)]
57. Fu, Y.; Mo, H.-Y.; Gao, W.; Hong, J.-Y.; Lu, J.; Li, P.; Chen, J. Affinity selection-based two-dimensional chromatography coupled with high-performance liquid chromatography-mass spectrometry for discovering xanthine oxidase inhibitors from *Radix Salviae Miltiorrhizae*. *Anal. Bioanal. Chem.* **2014**, *406*, 4987–4995. [[CrossRef](#)]
58. Tang, H.-J.; Zhang, X.-W.; Yang, L.; Li, W.; Li, J.-H.; Wang, J.-X.; Chen, J. Synthesis and evaluation of xanthine oxidase inhibitory and antioxidant activities of 2-arylbenzo[b]furan derivatives based on salvianolic acid C. *Eur. J. Med. Chem.* **2016**, *124*, 637–648. [[CrossRef](#)]
59. Tang, H.J.; Li, W.; Zhou, M.; Peng, L.-Y.; Wang, J.-X.; Li, J.-H.; Chen, J. Design, synthesis and biological evaluation of novel xanthine oxidase inhibitors bearing a 2-arylbenzo[b]furan scaffold. *Eur. J. Med. Chem.* **2018**, *151*, 849–860. [[CrossRef](#)]

60. Malik, N.; Dhiman, P.; Khatkar, A. In-silico design and ADMET studies of natural compounds as inhibitors of xanthine oxidase (XO) enzyme. *Curr. Drug Metab.* **2017**, *18*, 577–593. [[CrossRef](#)]
61. Malik, N.; Dhiman, P.; Khatkar, A. Mechanistic approach towards interaction of newly synthesized Hesperidin derivatives against xanthine oxidase. *Int. J. Biol. Macromol.* **2019**, *135*, 864–876. [[CrossRef](#)] [[PubMed](#)]
62. Narasimhan, B.; Sharma, D.; Kumar, P. Benzimidazole: A medicinally important heterocyclic moiety. *Med. Chem. Res.* **2012**, *21*, 269–283. [[CrossRef](#)]
63. Shah, K.; Chhabara, S.; Shrivastava, S.K.; Mishra, P. Benzimidazole: A promising pharmacophore. *Med. Chem. Res.* **2013**, *22*, 5077–5104. [[CrossRef](#)]
64. Nile, S.H.; Kumar, B.; Park, S.W. In Vitro Evaluation of Selected Benzimidazole Derivatives as an Antioxidant and Xanthine Oxidase Inhibitors. *Chem. Biol. Drug Des.* **2013**, *82*, 290–295. [[CrossRef](#)]
65. Hou, X.; Sun, M.; Bao, T.; Xie, X.; Wei, F.; Wang, S. Recent advances in screening active components from natural products based on bioaffinity techniques. *Acta Pharm. Sin. B* **2020**, *10*, 1800–1813. [[CrossRef](#)]
66. Nie, Y.L.; Wang, W.H. Immobilized Enzyme Reactor in On-line LC and Its Application in Drug Screening. *Chromatographia* **2009**, *69*, 5–12. [[CrossRef](#)]
67. de Moraes, M.C.; Temporini, C.; Calleri, E.; Bruni, G.; Ducati, R.G.; Santos, D.S.; Cardoso, C.L.; Cass, Q.B. Evaluation of capillary chromatographic supports for immobilized human purine nucleoside phosphorylase in frontal affinity chromatography studies. *J. Chromatogr. A* **2014**, *1338*, 77–84. [[CrossRef](#)] [[PubMed](#)]
68. Guo, J.; Lin, H.; Wang, J.; Lin, Y.; Zhang, T.; Jiang, Z. Recent advances in bio-affinity chromatography for screening bioactive compounds from natural products. *J. Pharm. Biomed. Anal.* **2019**, *165*, 182–197. [[CrossRef](#)]
69. de Moraes, M.C.; Cardoso, C.L.; Seidl, C.; Moaddel, R.; Cass, Q.B. Targeting Anti-Cancer Active Compounds: Affinity-Based Chromatographic Assays. *Curr. Pharm. Des.* **2016**, *22*, 5976–5987. [[CrossRef](#)] [[PubMed](#)]
70. Rodrigues, M.V.N.; Rodrigues-Silva, C.; Boaventura, S., Jr.; Oliveira, A.S.S.; Rath, S.; Cass, Q.B. On-Flow LC-MS/MS method for screening of xanthine oxidase inhibitors. *J. Pharm. Biomed. Anal.* **2020**, *181*, 113097. [[CrossRef](#)]
71. Rodrigues, M.V.N.; Corrêa, R.S.; Vanzolim, K.L.; Santos, D.S.; Batista, A.A.; Cass, Q.B. Characterization and screening of tight binding inhibitors of xanthine oxidase: An on-flow assay. *RSC Adv.* **2015**, *5*, 37533–37538. [[CrossRef](#)]
72. Rodrigues, M.V.; Barbosa, A.F.; da Silva, J.F.; dos Santos, D.A.; Vanzolini, K.L.; de Moraes, M.C.; Corrêa, A.G.; Cass, Q.B. 9-Benzoyl 9-deazaguanines as potent xanthine oxidase inhibitors. *Bioorg. Med. Chem.* **2016**, *24*, 226–231. [[CrossRef](#)] [[PubMed](#)]
73. Peng, M.-J.; Shi, S.-Y.; Chen, L.; Zhang, S.-H.; Cai, P.; Chen, X.-Q. Online coupling solid-phase ligand-fishing with high-performance liquid chromatography-diode array detector-tandem mass spectrometry for rapid screening and identification of xanthine oxidase inhibitors in natural products. *Anal. Bioanal. Chem.* **2016**, *408*, 6693–6701. [[CrossRef](#)] [[PubMed](#)]
74. Wang, Y.; Adeoye, D.I.; Ogunkunle, E.O.; Filla, R.T.; Roper, M.G. Affinity Capillary Electrophoresis: A Critical Review of the Literature from 2018 to 2020. *Anal. Chem.* **2020**, *93*, 295–310. [[CrossRef](#)]
75. Lin, P.; Zhao, S.; Lu, X.; Ye, F.; Wang, H. Preparation of a dual-enzyme co-immobilized capillary microreactor and simultaneous screening of multiple enzyme inhibitors by capillary electrophoresis. *J. Sep. Sci.* **2013**, *36*, 2538–2543. [[CrossRef](#)]